Fluctuating Radiocarbon Offsets Observed in the Southern Levant and Implications for Archaeological Chronology Debates

Sturt W. Manning, Carol Griggs, Brita Lorentzen, Christopher Bronk Ramsey,
David Chivall, A. J. Timothy Jull, Todd E. Lange

Supporting Information Appendix (SI Appendix)

1. Dendrochronology

Sections and cores of *Juniperus phoenicea* were sampled from timbers from former late Ottoman period structures of end 19th/early 20th century AD date incorporated into the historic Hotel Taybet Zaman (site code TZM) in Taybeh Village, southern Jordan (ref. 1 pp.33-34) (for brief discussion of the Taybet Zaman site, see below). Samples were sanded to a high polish for examination and measured to the nearest 0.001 mm on a measuring table under a stereomicroscope. Analysis and cross-dating between the samples followed standard dendrochronological methods (2-4). We employed the Tellervo TRiDaS v.1.3.0 dendrochronological analysis package for measurement (5), and Corina v.1.1 (6) and COFECHA (7) for crossdating and chronology building. The set of 10 tree-ring series comprising the TZM chronology is shown with their chronological placement and summary of crossdating statistics (calculated in Corina) in Fig. S1. The TZM chronology was crossdated and placed into absolute time from AD1610-1940, against an absolutely-dated *Juniperus phoenicea* reference chronology built from living trees from south Jordan (8, 9), which is available from the International Tree Ring Databank (ITRDB):
https://www1.ncdc.noaa.gov/pub/data/paleo/treering/chronologies/asia/jord001.crn with the individual raw data available from:
https://www1.ncdc.noaa.gov/pub/data/paleo/treering/measurements/asia/jord001.rwl. A summary of the crossdating statistics comparing the TZM site chronology with the reference chronology are shown in Fig. S2. The high internal correlation and visual and statistical similarities between TZM and the juniper reference chronology indicate that TZM is a robust crossdated chronology securely placed in calendar time. The tree-ring measurements for the 10 TZM samples are listed in Table S1 and have been submitted to the International Tree Ring Databank (http://www.ncdc.noaa.gov/data-access/paleoclimatology-data/datasets/tree-ring).

The tree-ring sequences selected for ^{14}C measurement were dissected with a steel blade under a binocular microscope. Sequences typically include 5 tree-rings (years) but in a few cases where

www.pnas.org/cgi/doi/10.1073/pnas.1719420115

the tree-rings were very narrow a longer sequence (larger number of tree-rings) was dated. The sequences and their corresponding ^{14}C data are listed in Table S2.

A second set of ^{14}C data are also available on a *Juniperus phoenicea* sample (BADG-1) found at a different locality ~19 kilometers away in southern Jordan (the locus area was code named BADG and is about 4km NNW of Al-Bayda) ~30°25'18"N, 35°26'58"E (Fig.1A). This sample came from a tree stump that had been cut some years prior to our visit to the location. Two other samples from this locus offer dated tree-ring sequences AD/CE 1559-1995 and 1619-2006 (BADG-4, BADG-3 respectively). The ^{14}C dates were run on samples cut, at that time, as approximately a time-series of consecutive 5-ring/year samples from BADG-1. In reality, the dendrochronology was not at all secure when this work was carried out, and a number of (narrow, partial and locally absent) rings were not then recognized. Thus the series is *not* known-age (contrast TZM), rather a relative ordered sequence, and, in particular, the real age span of the dated sequence is substantially longer than originally thought by, overall, ~50 years. The gaps between the mid-point of each sample dated should have been ~5 years, but in reality this is a minimum gap, and in a number of instances the gaps are in reality rather longer. The ordered sequence and the ^{14}C dates on the constituent samples are listed in Table S3. We do not refer to tree-rings for the reasons just outlined for the BADG-1 samples, rather we refer to the sample bag numbers from 1 (oldest, the innermost set of rings sampled) onwards. Hence BADG Bag 1, Bag 2 … etc., below.

2. Radiocarbon

TZM. The ^{14}C measurements on the *Juniperus phoenicea* samples were obtained via the ^{14}C Accelerator Mass Spectrometry (AMS) method at the Arizona Accelerator Mass Spectrometry Laboratory, University of Arizona (AA), and the Oxford Radiocarbon Accelerator Unit, University of Oxford (OxA). Where both laboratories ran samples of the same calendar (tree-ring) age, this material came from identical tree-ring samples. The tree-rings were prepared via standard ABA with a bleaching step (sodium hypochlorite) to holocellulose at Arizona in a modified Jayme-Wise process as shown to achieve good pretreatment characteristics (10-12), and either as ABA plus bleach samples or as α-cellulose samples, with or without a solvent extraction step, at Oxford (the different pretreatment regimes are indicated for the Oxford samples in Table S2) (13, 14) and then dated following standard procedures (10, 11, 15). Where the identical tree-rings were pretreated by different approaches at Oxford, especially TZM-4 AD1818-1822 and TZM-3 AD1888-1892, the results are indistinguishable (Table S2) – with the exception of OxA-29735, which is an outlier (^{14}C age is too recent), when compared with the three other measurements on this same sample (and OxA-29735 is not employed in the analyses). The general similarities among the differently pretreated Oxford data, and between the Arizona and Oxford data (and see also the BADG samples below) conform to the generally observed pattern in previous studies that only small differences in ^{14}C measurements usually derive from differing pretreatments ranging from ABA + bleach through to holocellulose to α-cellulose (16). The reported ^{14}C ages are conventional radiocarbon ages expressed as ^{14}C years Before Present (BP) employing the 5568 years Libby half-life and AD1950 as "present". The values have been corrected for isotopic fractionation using the $\delta^{13}C$ values measured on the AMS. The quoted $\delta^{13}C$ values in Table S2 were measured independently on a stable isotope mass spectrometer at each laboratory.

In the main text the Arizona and Oxford datasets are considered separately in comparisons versus IntCal13 (17): Fig. 2. We may also combine both data sets – thus pooling data for the identical samples from either or both laboratories where available into weighted average values (18). In all but one case the data are compatible with representing estimates of the same ^{14}C age within 95% probability (18). The solitary exceptions are the data centered at 1677 which narrowly fail a χ^2 test (T=4.191 > 3.8 for df2). Fig. S3 shows the combined TZM data set versus IntCal13 (see also Table S4). Figure S4 shows the overall average offset in ^{14}C ages between the combined Arizona and Oxford Jordanian samples and IntCal13 tested with a neutral prior of 0±20 ^{14}C years using the Delta_R function in OxCal (19): 18.6±2.5 ^{14}C years (for the OxCal runfile for this analysis, see Table S5). Of the 65 TZM data, 12 (18%) are not only offset from the IntCal mean value (Fig. S4A), but are incompatible as representing the same ^{14}C age allowing for errors on both the TZM data and IntCal13 within 95% probability (18): Table S4. In every case the relevant significantly different TZM ^{14}C age is older than the contemporary IntCal13 value. These are the data centered at 1627, 1717, 1722, 1727, 1750, 1770, 1885, 1890, 1895, 1900, 1905, 1910 (Table S4). Figure S4B shows the offset of the TZM data versus IntCal13 (linear interpolation) in terms of ΔZ values using the equation

$$\Delta Z = \frac{\text{TZM 14Csample} - \text{IntCal13 14Cvalue}}{\sqrt{(\text{TZM}\sigma\hat{}2 + \text{IntCal13}\sigma\hat{}2)}}$$

Where *ΔZ* is the normalized difference (Z-Score), TZM 14Csample and IntCal13 14Cvalue are the respective ^{14}C ages values of each TZM sample and the corresponding (linear interpolation) IntCal13 ^{14}C mean values, and TZMσ and IntCal13σ are the respective uncertainties (see Table S4). 74% of the data are > 0, 25% <0. One value = 0. The offset to older ages is clear.

As in Fig. 2, two approximate intervals stand out with most data involved offering offset ^{14}C ages (with the TZM ^{14}C data from Jordanian juniper wood older in these periods than contemporary IntCal13 ^{14}C data on Central and Northern European and North American wood), whereas at other times the picture is either mixed, or there is no substantive offset evident (Fig. S3). Fig. S5 shows the offset values from Fig. S3 with a range of smoothing curves through these data using 5, 7, 9 and 11 point adjacent averages, as well as 11 and 22 point LOESS (locally weighted scatter-plot smoother) curves. The two periods with mainly consistent larger offsets (evident in the raw data and in all smoothed curves), and noted in Fig. S3, are indicated. Fig. S6 shows the data on the TZM samples by individual tree sample employed for each ^{14}C date. This confirms that the offsets observed, especially those in the two periods of greater offset noted in Figs. 2, S3, S5, are represented in more than one tree sample, and so are not the product of one unusual tree.

BADG. The ^{14}C measurements on the BADG samples were also run at Arizona and Oxford and on the same basis as the TZM samples described above. We consider an ordered sequence of samples from (oldest) Bag 1 to (most recent) Bag 33. We stopped the sequence at Bag 33 because, after Bag 33, the BADG samples start in several cases in both the Arizona (from Bag 36) and Oxford (from Bag 35) measurements either to return modern, post-bomb, ^{14}C values in some cases, or they exhibit considerable variation in the ^{14}C values measured (from Bag 34 onwards in several cases) and with some of these ^{14}C ages likely affected by modern ^{14}C: see Table S3. Hence, rather than subjectively selecting what might appear to be the more acceptable results, we take the conservative view that from Bag 34 onwards there are issues with modern (likely remaining resin or lignin-associated) contamination that affect a number of these dates and so it is best to exclude all these dates from analysis. Where available, we employ the OxA dates starting 32XXX, rather than 29XXX, as these represent re-runs of the same samples but re-processed fully to α-cellulose after the issue of (apparently) very mobile bomb-age ^{14}C material became evident in a few of the more recent samples from the 29XXX series. We assume that remaining mobile resin-associated or remaining lignin material is the primary issue which has not been fully removed in all cases in the later part of the 29XXX series (20). Note: such a bomb-age/modern contamination issue, where and if relevant, would lead to incorrectly recent ^{14}C ages, and is thus the very opposite of the older ^{14}C age offset observed in the TZM and BADG series for some intervals in the 17th to 19th centuries AD/CE (as in Figs. 2A, S3, S5, S6). Hence, if we have missed any such contaminant issue, it would work against the finding of the offsets we report! Thus the fact we observe the ^{14}C offsets in the BADG series in the data from both the Arizona and Oxford laboratories in the 17th-19th centuries AD/CE indicates that these samples are not affected by bomb-age ^{14}C. We also highlight that this bomb-age issue just discussed for the BADG samples is totally irrelevant to the TZM samples because the constituent TZM trees had been felled and incorporated into a building before the bomb-era, and thus no possible bomb-age ^{14}C was ever incorporated into the cellulose of those samples.

When the BADG-1 samples were cut up, it was thought that there were ~5 rings/years in each sample and thus the mid-points of each sample were approximately 5 years apart. As noted above, this was not in reality the case, and a number of rings were either not recognized at that time or were missing (locally absent). Subsequently, a crossdated tree-ring chronology has been constructed from a couple of the BADG samples, but these ^{14}C BADG-1 samples had already been dissected and dated. (We note the obvious, for the benefit of readers: the history of the BADG-1 samples and its ^{14}C date series reflects an original, mistaken, belief that we had a secure dendrochronology for this sample, and so the set of samples were cut and the ^{14}C dates run as reported in Table S3. It was then realized that the dendrochronology was invalid and the other BADG samples were re-studied and a long secure dendrochronology achieved from BADG-3 and BADG-4 (AD/CE 1559-2006) that crossdates with both TZM (AD/CE 1610-1940: Figs.1B, S1) (t=6.7, r=0.35) and strongly with the previous Jordan juniper chronology (8, 9) AD/CE 1469-1995 (t=14.03, r=0.56) (6). The original aim or hope was, of course, for the BADG-1 dataset to offer a parallel dataset versus TZM. But this is impossible as the dataset we had acquired comprised an ordered series of samples and so ^{14}C dates, but *not* a secure known-age time-series. Hence only the TZM data are employed in the main text. Nonetheless, as we discuss in the next paragraph, we can still employ the BADG-1 ordered sequence to consider the question of a ^{14}C offset versus the IntCal13 calibration dataset, and hence partly 'rescue' this BADG-1 dataset and a past mistake, and make these data at least partially useful as strong independent evidence supporting the scale and approximate placement of the offsets reported from the TZM dataset.)

The BADG Bag 1 to Bag 33 sequence employed includes 29 comparisons of the same sample between Arizona (AA) and Oxford (OxA) and only in two cases are the data incompatible at the 95% level (18): Fig. S7. The BADG ordered sequence can be compared against IntCal13 (17) as a Sequence with gaps in OxCal (19). The question is the appropriate gap (and error on this estimate) to allow for between each sample, since we know there were errors and likely under-estimates in a number of cases concerning rings recorded. We allow for a likely conservative range of error estimates from 0-40%, 0-60% and 0-80% as allowing for the plausible range of error involved and likely including the correct estimate. Thus we use gaps of 5±2 years, 5±3 years and 5±4 years between samples in three different models. (To explain: the general issue with the initial work on the BADG-1 sample was a failure to recognize some, very narrow, tree-rings and locally absent rings – not usually over-counting tree rings – thus we regard the original ~5 years as the *minimum* gap between the dissected sample series, but, allowing for possible mistakes also with false rings or other errors, we in addition allow an error of ±2 or ±3 or ±4 years on each of those minimum 5 year gaps to try to realistically accommodate all plausible errors). We employ the weighted average of the Arizona and Oxford dates for each sample where satisfactory (18) and for the two exceptions, samples Bag 1 and Bag 8, we consider these dates separately within a Phase (Bag 1, Bag 8) within the Bag 1 to Bag 33 OxCal Sequence. Since these two exceptions (Bag 1, Bag 8) both occur at times of rapidly changing atmospheric ^{14}C levels (steep slopes on the ^{14}C calibration curve), it may be that in one or both of these cases not exactly the same tree-rings were in fact dated, for example with a slight bias to one or a couple of older and/or more recent tree-rings between the samples and this might have exaggerated the different dates obtained. We tested for the existence, or not, of an average ^{14}C offset between these dates on the BADG-1 Jordanian juniper ordered sequence and those from the data comprising the IntCal13 calibration dataset (17) (from wood from Central and Northern Europe and North America) employing a Delta_R query in OxCal (19) with the IntCal13 curve resolution set at 5 years with a neutral prior of 0±20 (we employ a 5 year curve resolution in this case, versus the 1-year in the main text, because of the much more loosely constrained data in the BADG-1 case in order to avoid a very noisy, if nonetheless overall similar/compatible, outcome with a 1-year curve resolution): Figs. S8-S13. The OxCal runfile is listed in Table S6. We note that we report examples of models which either achieved single (non-ambiguous) 68.2% probability ranges or we report the clearly most likely sub-range (e.g. >45% of total probability from the most likely 68.2% range in some cases) – since various runs offered alternative ranges (with the approximate range indicated in Figs. S8-S10 nonetheless including the most likely of the multiple ranges calculated in any such cases). Although there is more noise in the analysis as the potential error on the gap increases, from ±2 to ±4 years (40%-80%), the likely best fit remains very similar: Figs S8-S10. We therefore make further comments based on the 5±2 years gap model – which we also believe likely best represents the real situation. The data exhibit an offset with a most likely 68.2% probability range of (rounded) ~26±9 years (Fig. S11). If a neutral prior of 0±10 is employed the offset reported (most likely 68.2% range) is ~23±5 ^{14}C years: Fig. S14. This is a similar finding to the TZM analysis in the main text and offers some independent confirmation of the ^{14}C offsets reported from a different tree sample. The best placement of the BADG-1 dataset against IntCal13 (Fig. S8) shows that – as in the case of the TZM data (Fig. 2) – a number of the BADG ^{14}C ages are older than the corresponding IntCal13 values. We then re-ran the BADG Bags 1-33 Sequence in Fig. S8 with the Delta_R values of both 26±9 ^{14}C years and 23±5 ^{14}C years and with the calibration curve (IntCal13) resolution set at 5 years. The models now show a reasonably good fit, returning respective satisfactory or near-satisfactory OxCal Amodel values of ~71.8 and ~49.1 and Aoverall values of ~62.9 and ~48.4 and the posterior densities for the calculated offsets, in dark gray, now correspond well with the assumed values, in light gray, confirming in reverse the existence of the offset at, on average, the stated level (Figs. S15, S16). We also show the 26±9 ^{14}C years case re-run with calibration curve resolution set at 1 year for comparison – it is very similar (Fig. S17). This ordered sequence of BADG data from a different tree and a different site ~19 kilometers away from TZM in southern

Jordan, although not known-age, nonetheless clearly provides valuable (if imperfect) independent confirmation of the time varying ^{14}C offsets reported in the main text from the TZM samples (Figs. 2, S3). It is evident from Figs. S8-S10 that these offsets vary over time, and, comparing Figs. S8-S10 with Figs. 2, S3 and S5, we may observe that the periods of larger apparent offsets are similar in both the TZM and BADG series.

Quality Controls. A routine known-age sample testing program is run at the Oxford Laboratory to assess on-going dating accuracy (previous details in refs. 14, 21, 22). During the period when the main set of samples dated in this project were run at Oxford (2014-03-14 to 2016-11-04; dates OxA-29389 to OxA-34708 – four dates were run subsequently: OxA-35658, 35659, 36013, 36014), a total of 312 measurements were made on samples of known age wood and these indicate that 97.4% of dates were within 2σ with a systematic bias of 2.6±1.6 yr. As noted in the main text, we may also compare published data from Oxford on other known-age tree rings in the period AD/CE 1160 to 1660 (23, 24). These indicate a negligible offset ($\mu \pm \sigma$) from 48 data points of 3.38 ± 4.96 ^{14}C years versus IntCal13 (Fig. 3B, 3C), highlighting the real and substantial nature of the offset observed by the Oxford laboratory for the Jordanian juniper. A set of Oxford measurements on known age German Oak samples as employed in the IntCal13 dataset (17) offers another comparison (25). These data match the IntCal13 curve closely: Fig. S18. The mean offset testing with a neutral Delta_R of 0±10 ^{14}C years in OxCal (19) is effectively zero at 0.7±7.2 ^{14}C years (Fig. S19). The comparisons in Figs. 3B, 3C, S18 and S19 and other studies (26, 27) provide good grounds to regard the Oxford AMS ^{14}C data as compatible with other laboratories and with the IntCal13 dataset and the modelled IntCal13 calibration curve (and hence there is no substantive laboratory offset). Arizona continuously monitors accuracy by comparison of oxalic-I and oxalic-II during every run, and uses these data to increase the quoted error where needed. As noted in the text, recent high-precision inter-laboratory work demonstrates the accuracy and precision of the Arizona laboratory within stated error estimates (28, 29). Details of the calculations at Arizona are given in previous statements (30, 31).

Tel Rehov and Khirbat en-Nahas dates. The Tel Rehov ^{14}C dates and calendar age modelling reported in Fig. 4 were taken from the ^{14}C ages listed for the 11 archaeological elements shown in Fig. 2 of ref. 32. They were considered as a Sequence in OxCal 4.3 (19) with runs made with the ^{14}C data as published with IntCal13 (17) with curve resolution set at 5 years and then with an adjustment for a Delta_R value of 19±5 ^{14}C years, or use of the approximate Jordan juniper modified calibration curve (based on the patterns of offsets in Figs. S2, S3, S5) as shown in Fig. 4A: see Table S7. The published Khirbat en-Nahas set of ^{14}C data and Bayesian chronological model (33) were re-run comparing the calendar age ranges obtained from IntCal13 (17) with curve resolution set at 5 years versus those obtained if the ^{14}C values were adjusted by 19±5 ^{14}C years, or if the approximate Jordanian juniper (JJ) modified curve is used: see Table S8.

3. Red Sea coral dataset and Northern Hemisphere extra-tropical temperature records

The Red Sea coral $\delta^{18}O$ dataset (34) in Figure 2B is employed from:
https://www1.ncdc.noaa.gov/pub/data/paleo/coral/red_sea/felis2000_noaa.txt

In the main text we cited one recent discussion and analysis for the reconstruction of extra-tropical Northern Hemisphere temperature (35), which shows, in general: (i) a warming trend from around and in the half century or so following the peak Maunder Minimum period (the peak Maunder Minimum is dated ~AD1645-1700 (36)) – we observe a ^{14}C offset period ~1685-1762 (Fig. 2, Fig. S3) which largely corresponds to this post-peak Maunder Minimum and subsequent change period and also to an observed long, stable, wetter period (~1700-1750) in much of the Mediterranean (37); (ii) a warming trend for the period from the (post-Tambora) earlier/mid-19th century AD; and (iii) some correlation of these trends with changes in reconstructed total solar irradiance. Other recent work (38-41) for the Northern Hemisphere over the second millennium AD offers broadly consonant indications. The study of Mann (42) addressing the Middle East, while noting caveats for reconstructions for pre-20th century AD period, also reconstructs generally warmer conditions for the Middle East in the mid-19th century.

4. Taybet Zaman

The Taybet Zaman village site represents an interesting, if not uncontroversial, example of attempts to re-use elements of Jordan's heritage as part of the modern tourism industry. The entire town was leased by Jordan Tourism Investments and reused/transformed into a luxury hotel and tourist attraction. The positively recounted version has the local mayor, Abu Firas, of what by the start of the 1990s was a largely abandoned village with only a handful of families and their animals, meeting with Jordanian businessmen, and then selling the idea for the villagers to rent out the old village which these investors would restore and transform, go live in a new village with modern amenities, and have work if they wanted at the new hotel-resort to be constructed in the restored old village (e.g. http://www.independent.co.uk/travel/news-and-advice/tourism-must-be-small-to-be-kind-5366036.html). However, while noted as an example of re-use of historic structures (ref. 43 p.305), and a winner of a 1996 tourism for tomorrow award (ref. 44 p.180), aspects of this development and economic model for the site (and other such heritage re-use developments) are reviewed and critiqued less positively in other accounts (1, 45, 46), which note that these reclamations and developments are undertaken as a specialized activity by a (remote, not associated) intellectual and economic elite, and lead often to "gentrification and alienation of the host communities rather than a "revitalization" of their social and economic life or the reaffirmation of a sense of belonging to a shared place" (ref. 46 p.13). In practical terms for our project, the site (originally and still as restored) utilizes numerous *Juniperus phoenicea* timbers in its structures. Fig. S20 shows some examples of such timbers used in doors, doorways, roof beams, etc. at the time we sampled. Our sampling happened during renovations in 2011 and 2012. The site is now the Hyatt Zaman Hotel & Resort.

	TZM-1 1742- 1918 177									
TZM-12 1737- 1921	t=3.19 r=0.23 tr=62.2% n=177	**TZM-12 185**								
TZM-15 1610- 1910	t=4.12 r=0.30 tr=62.8% n=169	t=3.80 r=0.28 tr=57.8% n=174	**TZM-15 301**							
TZM-16 1638- 1810	t=9.56 r=0.76 tr=69.1% n=69	t=1.92 r=0.22 tr=58.2% n=74	t=3.88 r=0.28 tr=61.3% n=173	**TZM-16 173**				**Average t=5.79 r=0.46 tr=63.7%**		
TZM-17 1815- 1918	t=4.98 r=0.44 tr=64.6% n=104	t=5.16 r=0.45 tr=63.6% n=104	t=2.69 r=0.27 tr=52.1% n=96	n=0	**TZM-17 104**					
TZM-23 1754- 1940	t=7.69 r=0.52 tr=73.2% n=165	t=4.17 r=0.31 tr=60.8% n=168	t=3.05 r=0.24 tr=60.3% n=157	t=10.04 r=0.80 tr=76.8% n=57	t=4.26 r=0.39 tr=57.8% n=104	**TZM-23 187**				
TZM-3 1765- 1913	t=6.10 r=0.45 tr=66.2% n=149	t=6.86 r=0.49 tr=68.9% n=149	t=6.94 r=0.50 tr=63.8% n=146	t=4.42 r=0.55 tr=50.0% n=46	t=5.11 r=0.46 tr=60.2% n=99	t=7.16 r=0.51 tr=65.2% n=149	**TZM-3 149**			
TZM- 33&36 1799- 1934	t=5.83 r=0.47 tr=67.6% n=120	t=4.06 r=0.35 tr=59.4% n=123	t=3.88 r=0.35 tr=56.3% n=112	t=0.41 r=0.13 tr=31.8% n=12	t=5.59 r=0.48 tr=60.2% n=104	t=5.34 r=0.42 tr=67.4% n=136	t=5.35 r=0.45 tr=66.7% n=115	**TZM- 33&36 136**		
TZM-4 1719- 1912	t=5.87 r=0.41 tr=61.5% n=171	t=7.29 r=0.48 tr=66.9% n=176	t=6.86 r=0.45 tr=66.2% n=192	t=2.97 r=0.30 tr=58.8% n=92	t=4.99 r=0.45 tr=59.8% n=98	t=3.89 r=0.30 tr=66.1% n=159	t=7.35 r=0.52 tr=70.7% n=148	t=6.00 r=0.49 tr=59.3% n=114	**TZM-4 194**	
TZM-9 1822- 1911	t=7.00 r=0.60 tr=71.9% n=90	t=7.96 r=0.65 tr=73.0% n=90	t=10.05 r=0.73 tr=71.6% n=89	n=0	t=5.32 r=0.49 tr=62.9% n=90	t=4.52 r=0.43 tr=71.9% n=90	t=9.36 r=0.71 tr=75.8% n=90	t=6.32 r=0.56 tr=63.5% n=90	t=17.84 r=0.89 tr=75.3% n=90	**TZM-9 90**

Fig. S1. Internal crossdating of the Taybet Zaman (TZM) tree-ring chronology (Fig. 1B). Dendrochronological crossdating was evaluated using the following statistical parameters shown above: Student t-values (*t*) (47), Pearson correlation coefficient (*r*), and trend coefficient (*tr*) (48, 49) were calculated using the Corina v.1.1 software package (6); the number of years overlap (*n*) between the compared tree-ring series is also shown. The set of 10 trees offer a robust tree-ring chronology following standard dendrochronological procedures (2-4).

	TZM.CRN 1610-1940	
Jordan Juniper 1469-1995; R. Touchan (ITRDB)	t=14.54 r=0.63 tr=72.0% n=331	**Jordan Juniper n=527**

Fig. S2. Crossdating of the combined (master) Taybet Zaman (TZM) *Juniperus phoenicea* chronology in Fig. S1 against the existing southern Jordan *Juniperus phoenicea* chronology (8, 9) available from the International Tree Ring Databank (ITRDB): https://www1.ncdc.noaa.gov/pub/data/paleo/treering/chronologies/asia/jord001.crn with the individual raw data available from: https://www1.ncdc.noaa.gov/pub/data/paleo/treering/measurements/asia/jord001.rwl. The values indicate secure crossdating and hence secure absolute dates for the TZM chronology.

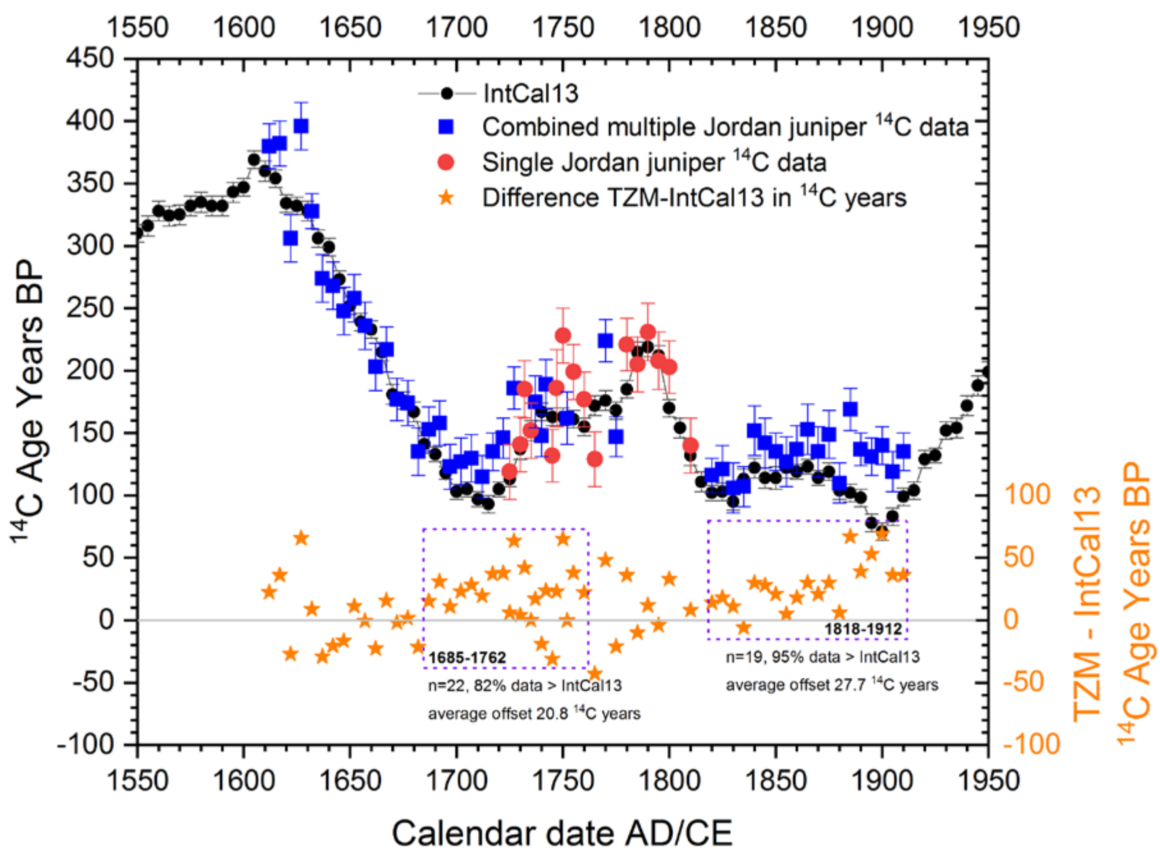

Fig. S3. The known-age placement of the pooled Oxford and Arizona TZM ^{14}C data (18) versus IntCal13 (17). Where there are two or more constituent TZM data, the symbol is blue, where there is only one ^{14}C date available the symbol is red. The difference in ^{14}C ages, TZM minus IntCal13, is shown below (see also Fig. S5). 1σ error bars shown. Of the 65 TZM data, 12 (18%) are not only offset from the IntCal mean value (Fig. S4), but are incompatible as representing the same ^{14}C age allowing for errors on both the TZM data and IntCal13 within 95% probability (18). These are the data centered at 1627, 1717, 1722, 1727, 1750, 1770, 1885, 1890, 1895, 1900, 1905, 1910. In every case the TZM ^{14}C age is older than the contemporary IntCal13 value. See Table S4.

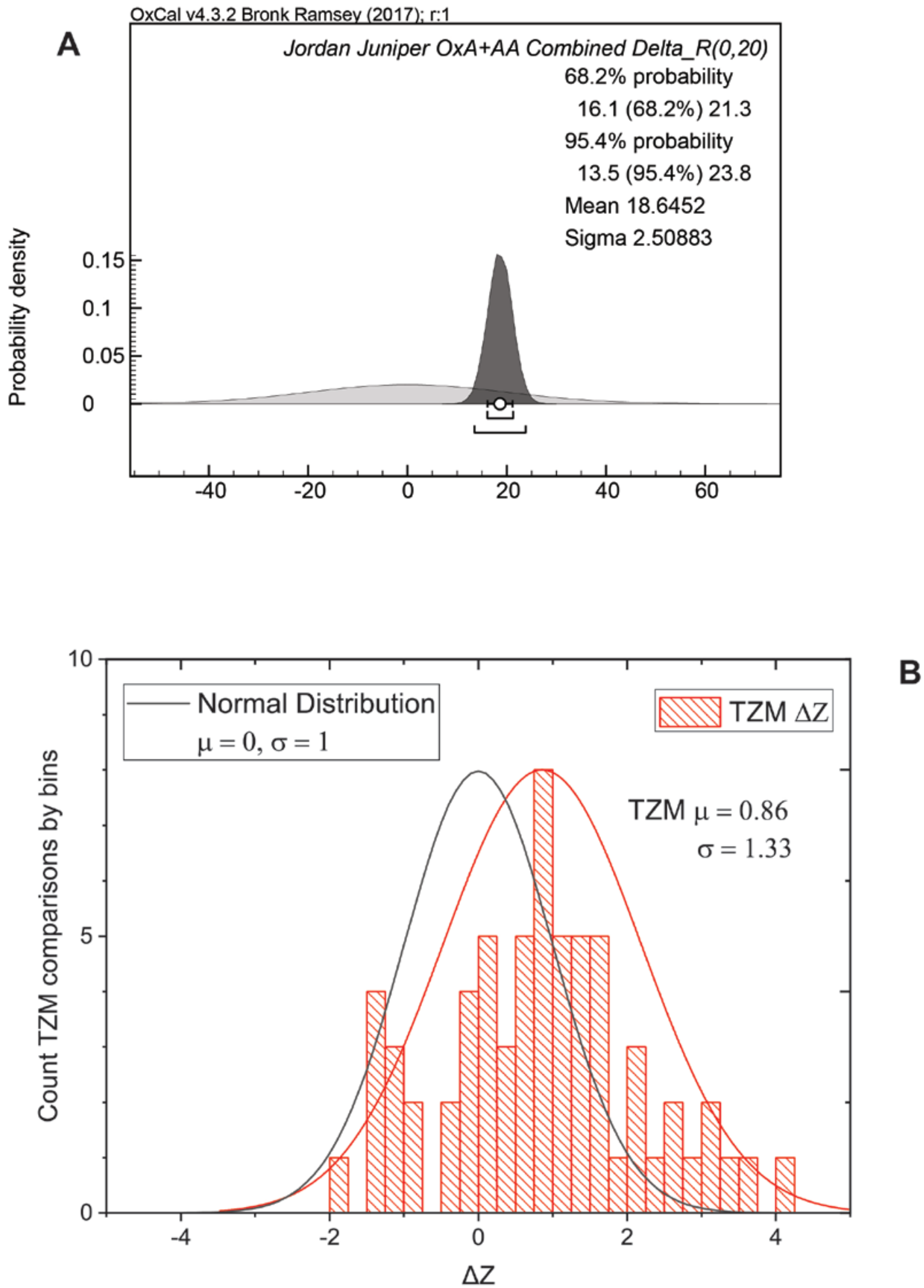

Fig. S4. A: the average offset for the pooled dataset in Fig S3, calculated as a Delta_R query in OxCal 4.3 (19) versus IntCal13 (17) with curve resolution set at 1 year with a neutral prior of 0±20. This yields a posterior of 18.6±2.5 ^{14}C years. B: The distribution of the normalized differences (ΔZ or Z scores) between the ^{14}C ages for each AA+OxA pooled (where possible) value versus IntCal13 including respective errors (Fig. S3, Table S4) and compared to a normal distribution with mean 0 and standard deviation 1.

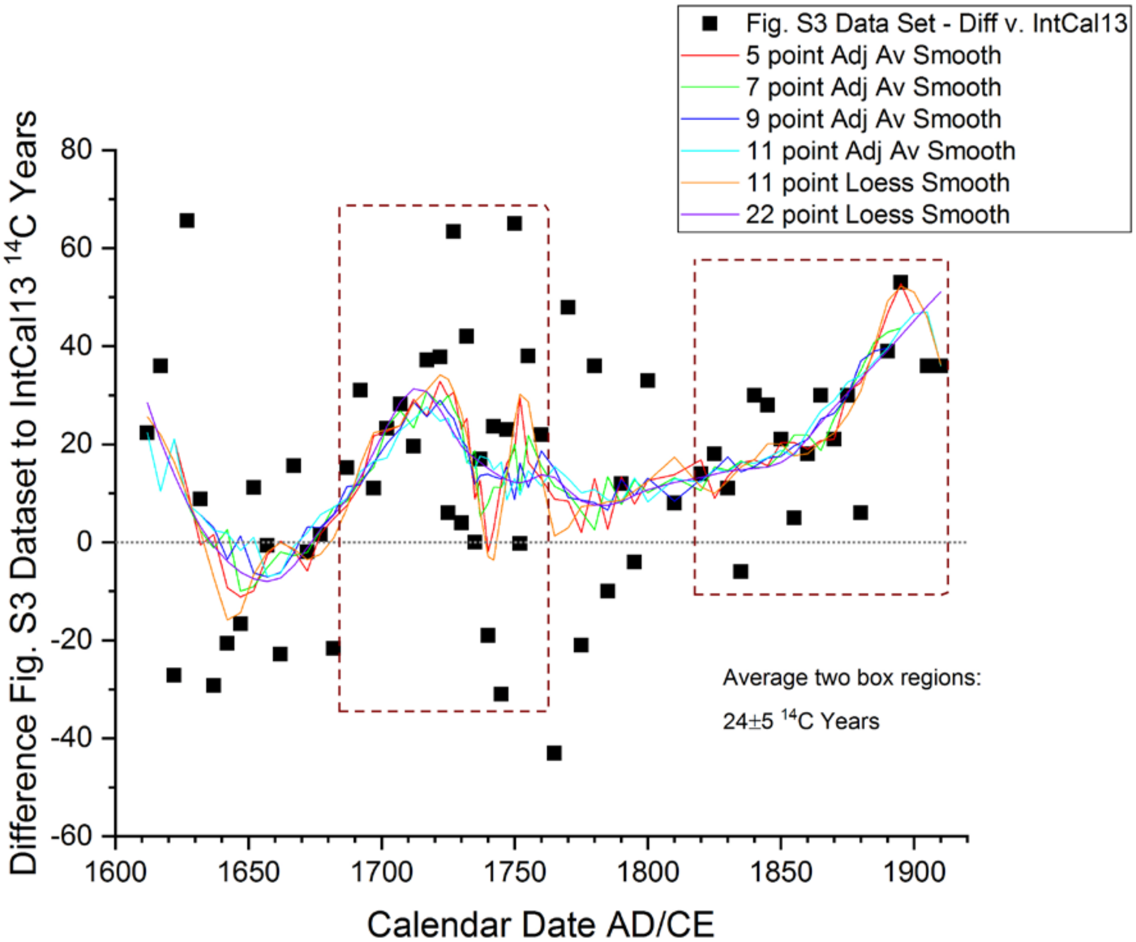

Fig. S5. The difference between the dataset from Fig. S3 versus IntCal13 (17), with four different adjacent average smoothed curves plotted through the data and also two locally weighted scatterplot weighting (Loess) curves. The offset fluctuates over time. The average offset in the two periods of greater largely sustained offsets, indicated by the dashed line boxes, is 24±5 ^{14}C years. The offset is ≥ +10 ^{14}C years for 63% of the comparisons.

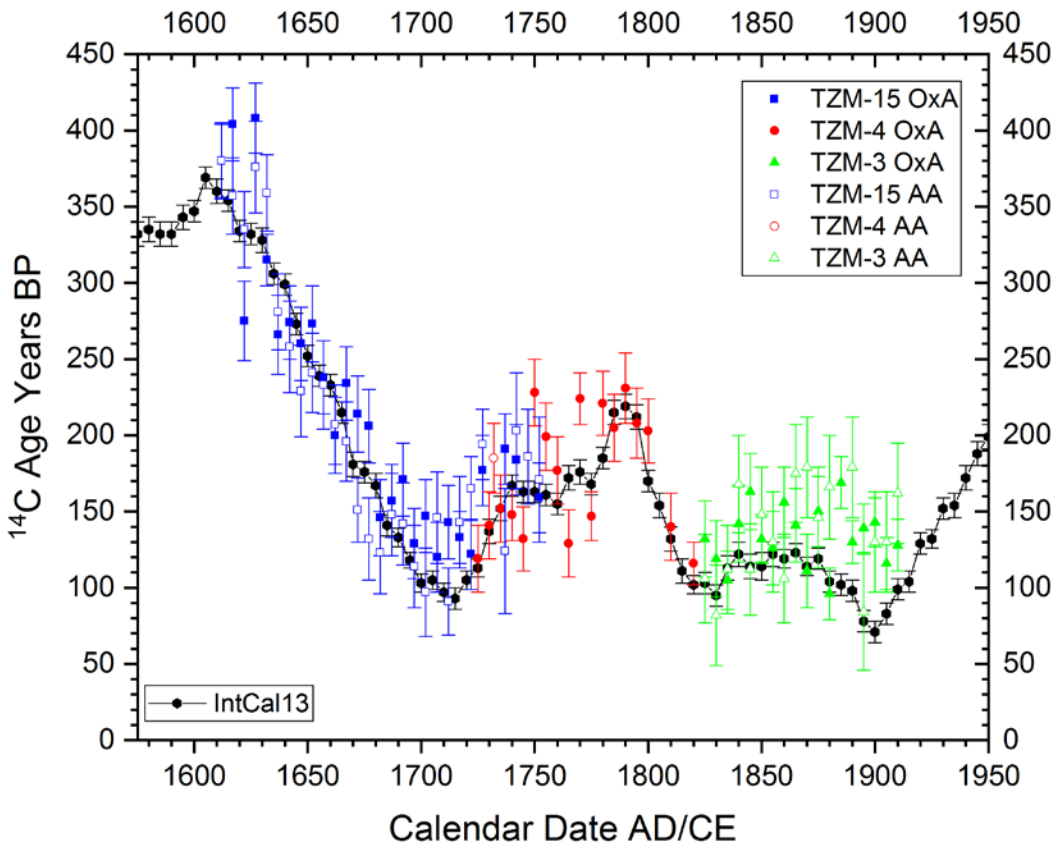

Fig. S6. The TZM ^{14}C date series, from the data in Table S2, and as shown in Fig. 2A, but indicating which data came from which of the three TZM tree samples (TZM-3, TZM-4 and TZM-15) employed in this study. 1σ error bars are shown.

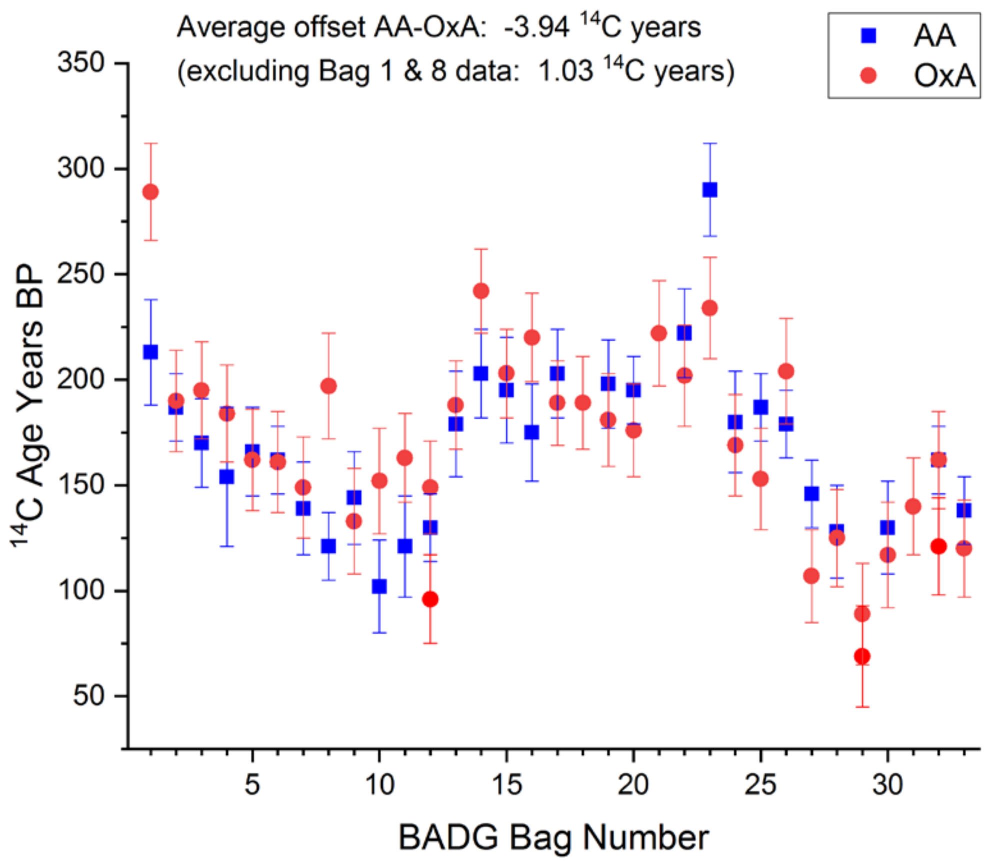

Fig. S7. ^{14}C data on the BADG samples from Bag 1 (oldest) to Bag 33 (most recent). 1σ error bars are shown.

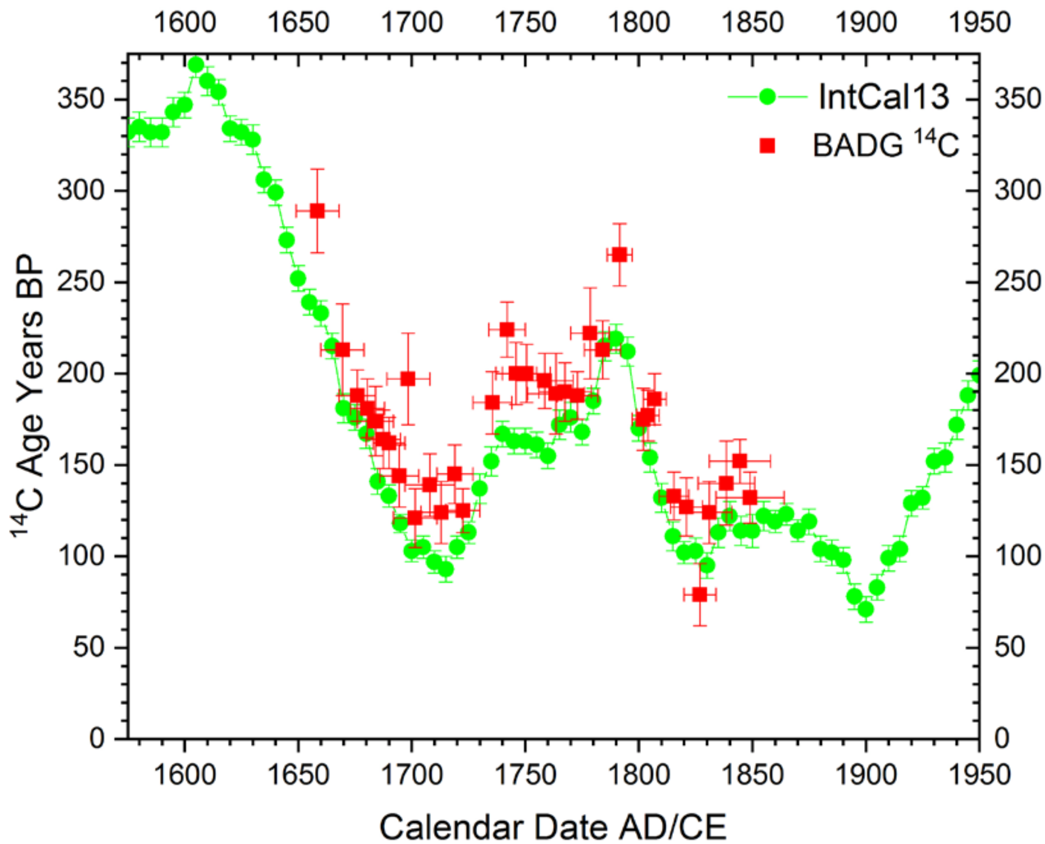

Fig. S8. The 68.2% most likely probability (highest posterior density = hpd) calendar age range fits of the BADG Bags 1 (oldest) to 33 (most recent) ordered ^{14}C sequence against IntCal13 with a minimum 5±2 years gap between the samples and allowing for a possible offset between the BADG Jordan juniper data and the IntCal13 (17) curve via a Delta_R query in OxCal (19) with a neutral prior of 0±20 (see Fig. S11). All error bars indicate 68.2% probability ranges. We employed a 5 year curve resolution. For the OxCal runfile, see Table S6. All but two of the BADG ^{14}C data lie above (older than) the corresponding IntCal13 mean value.

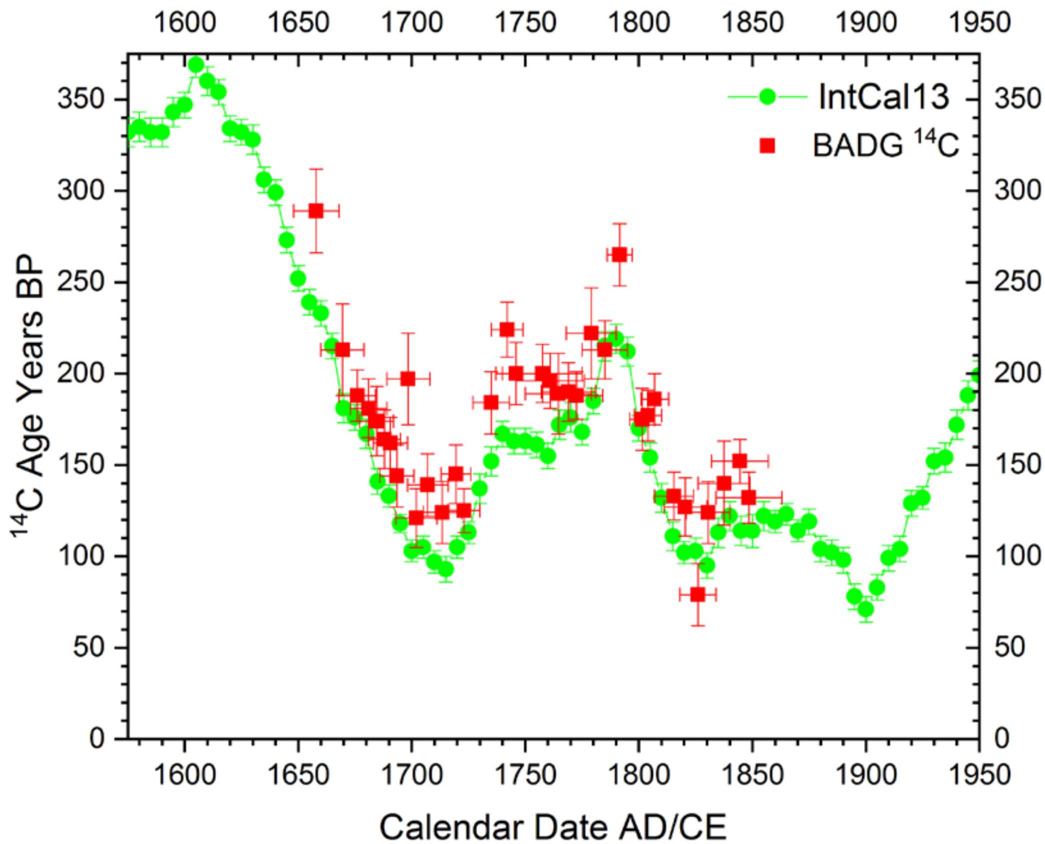

Fig. S9. The 68.2% most likely probability (highest posterior density = hpd) calendar age range fits of the BADG Bags 1 (oldest) to 33 (most recent) ordered ^{14}C sequence against IntCal13 with a minimum 5±3 years gap between the samples and allowing for a possible offset between the BADG Jordan juniper data and the IntCal13 (17) curve via a Delta_R query in OxCal (19) with a neutral prior of 0±20 (see Fig. S12). All error bars indicate 68.2% probability ranges. We employed a 5 year curve resolution. For the OxCal runfile, see Table S6. All but two of the BADG ^{14}C data lie above (older than) the corresponding IntCal13 mean value.

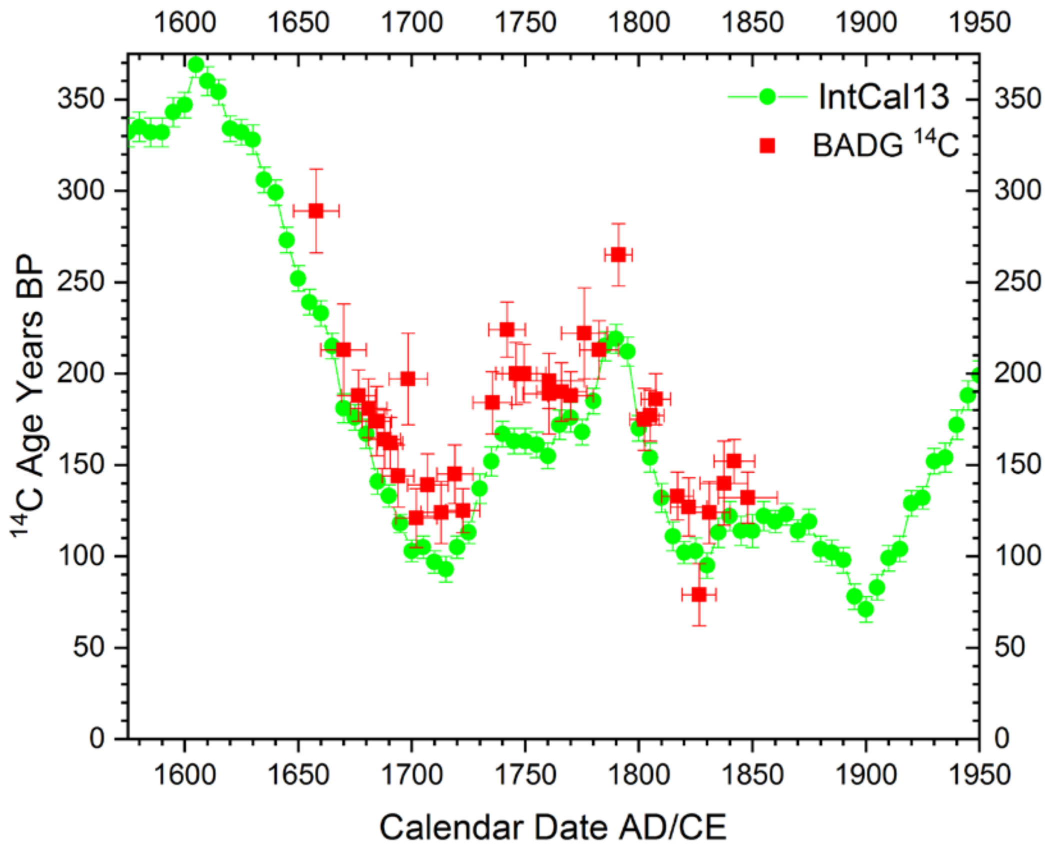

Fig. S10. The 68.2% most likely probability (highest posterior density = hpd) calendar age range fits of the BADG Bags 1 (oldest) to 33 (most recent) ordered ^{14}C sequence against IntCal13 with a minimum 5±4 years gap between the samples and allowing for a possible offset between the BADG Jordan juniper data and the IntCal13 (17) curve via a Delta_R query in OxCal (19) with a neutral prior of 0±20 (see Fig. S13). All error bars indicate 68.2% probability ranges. We employed a 5 year curve resolution. For the OxCal runfile, see Table S6. All but two of the BADG ^{14}C data lie above (older than) the corresponding IntCal13 mean value.

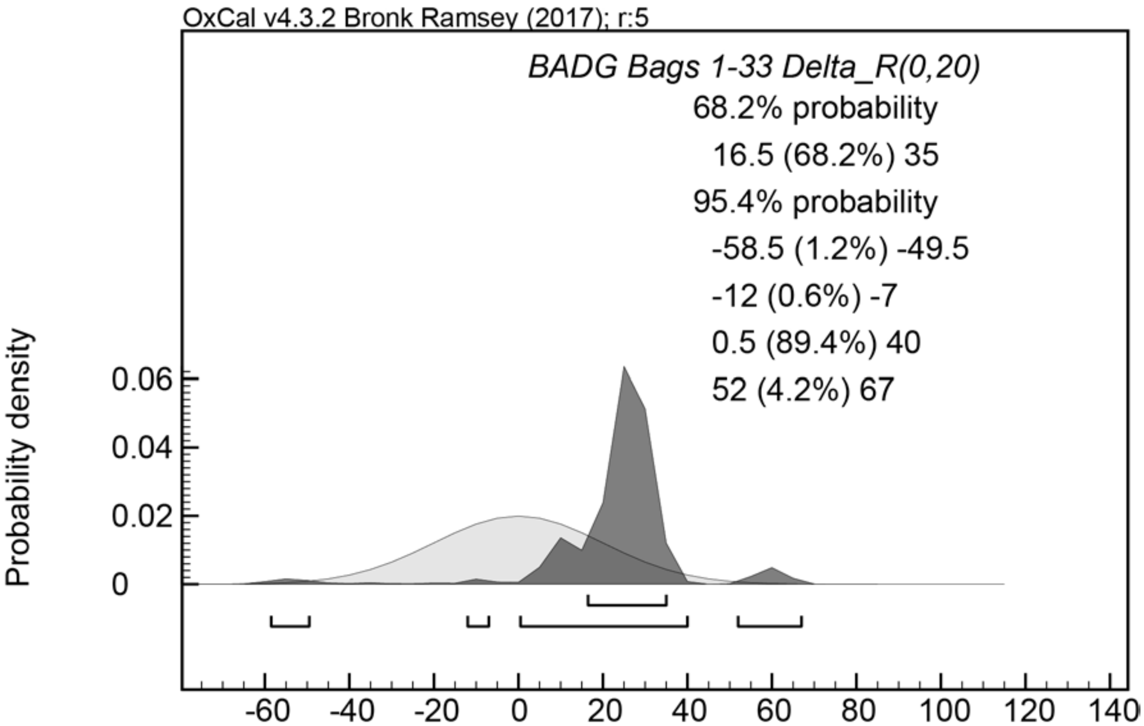

Fig. S11. The overall (average) offset (posterior density) between the BADG ^{14}C ages as best placed in Fig. S8 versus the IntCal13 (17) curve via a Delta_R query in OxCal (19) with a neutral prior of 0±20 ^{14}C years. The range of the most likely 68.2% probability region of the posterior is ~26±9 ^{14}C years.

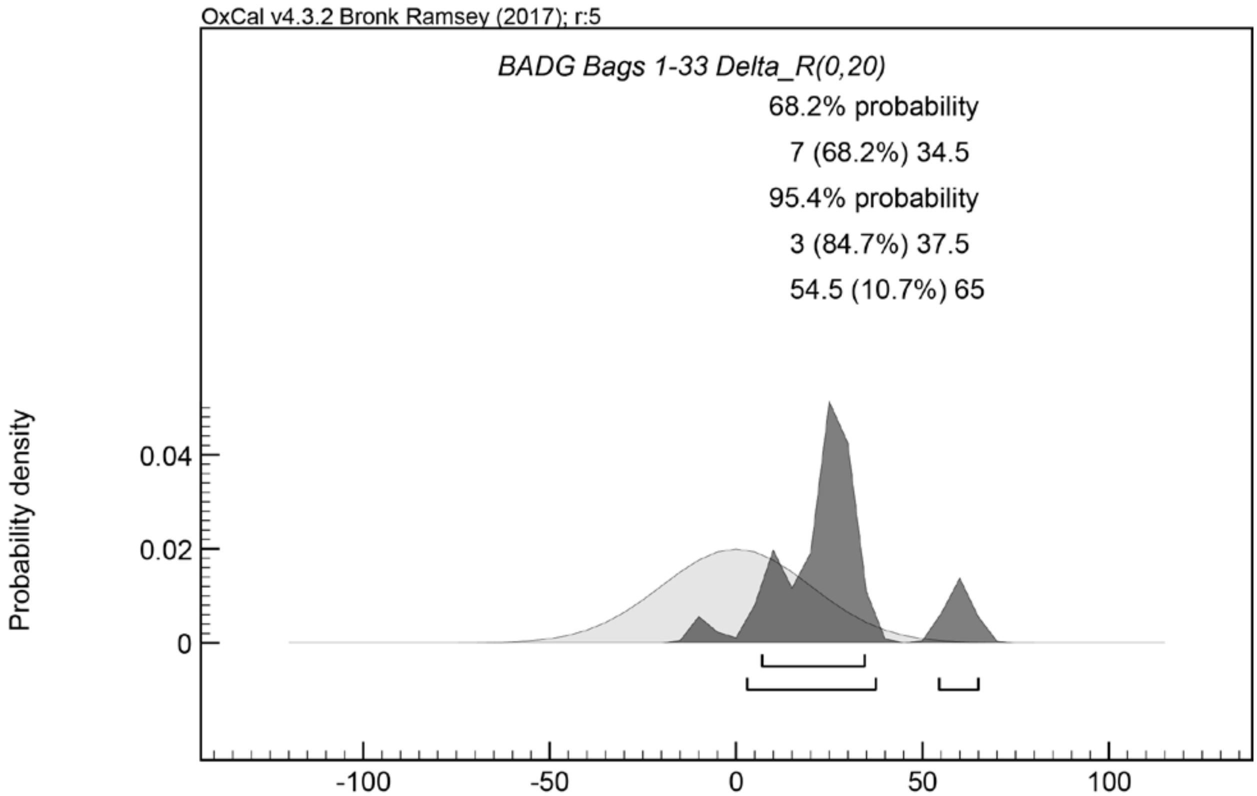

Fig. S12. The overall (average) offset (posterior density) between the BADG ^{14}C ages as best placed in Fig. S9 versus the IntCal13 (17) curve via a Delta_R query in OxCal (19) with a neutral prior of 0±20 ^{14}C years. The range of the most likely 68.2% probability region of the posterior is ~20±13.75 ^{14}C years.

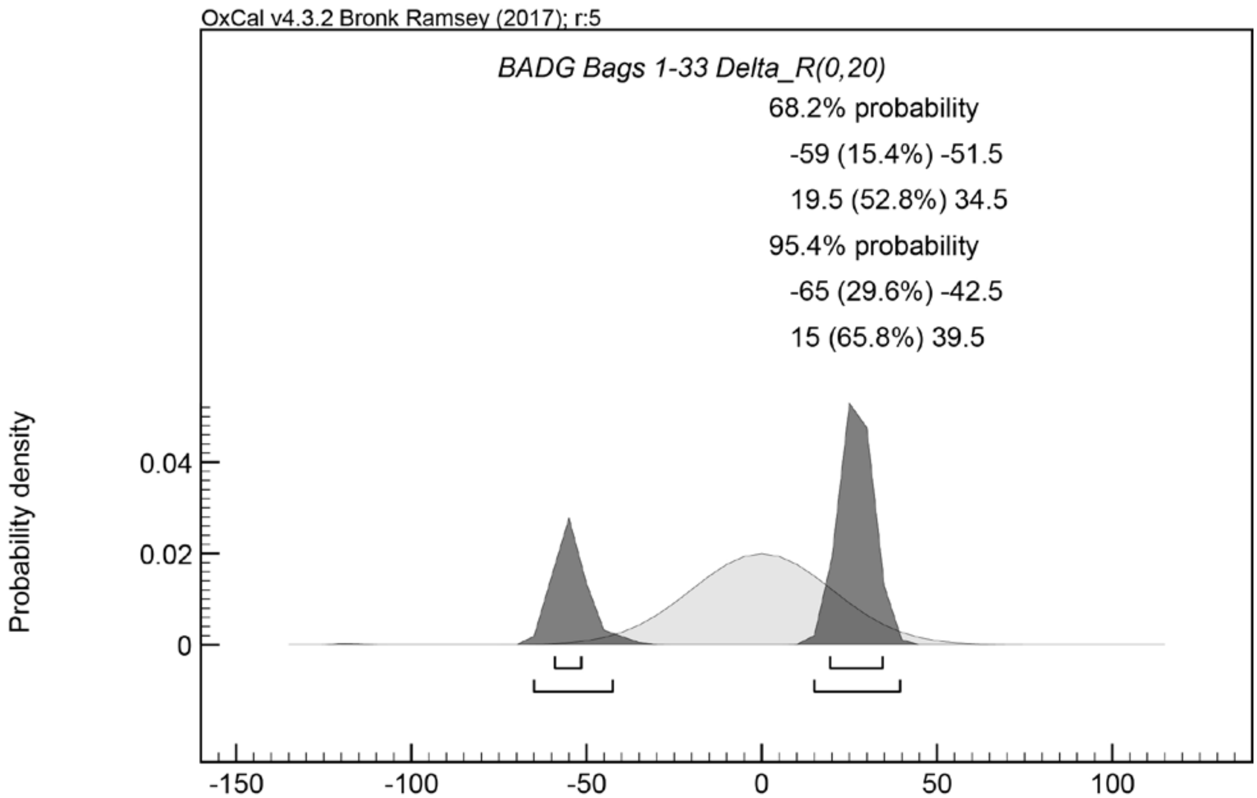

Fig. S13. The overall (average) offset (posterior density) between the BADG ^{14}C ages as best placed in Fig. S10 versus the IntCal13 (17) curve via a Delta_R query in OxCal (19) with a neutral prior of 0±20 ^{14}C years. A split range, as shown, is typical, but with a clear most likely solution. The much less likely alternative solution tries to place the entire BADG bags 1-33 series within the 17th century. This appears impossible in practical terms, considering (i) the approximate tree-ring sequence information which in fact underestimated, not massively over-estimated, the ring count, so bags 1-33 contain probably no less than around 165 rings/years and likely rather more given under-counting, and (ii) samples from the post bag 33 BADG series, starting from bag 35, included samples with post-bomb ^{14}C, so bag 33 cannot be 17th century when bag 33 is only supposedly ca.10 rings plus or minus counting errors before bag 35. A placement at least in the mid-later 19th century seems the earliest possible date that makes sense for bag 33. The range of the most likely sub-region of the 68.2% probability region of the posterior is ~27±7.5 ^{14}C years.

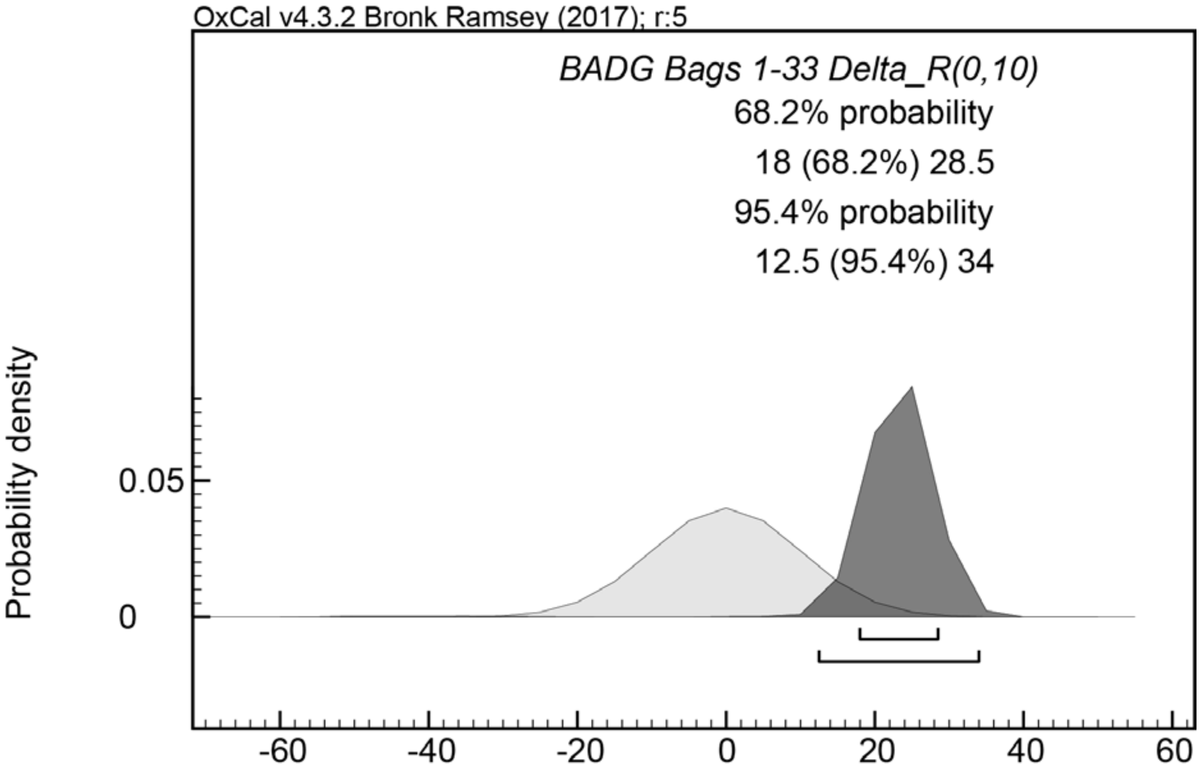

Fig. S14. As Fig. S11 but with the neutral prior of 0±10 ^{14}C years. The range of the most likely 68.2% probability region of the posterior is ~23±5 ^{14}C years.

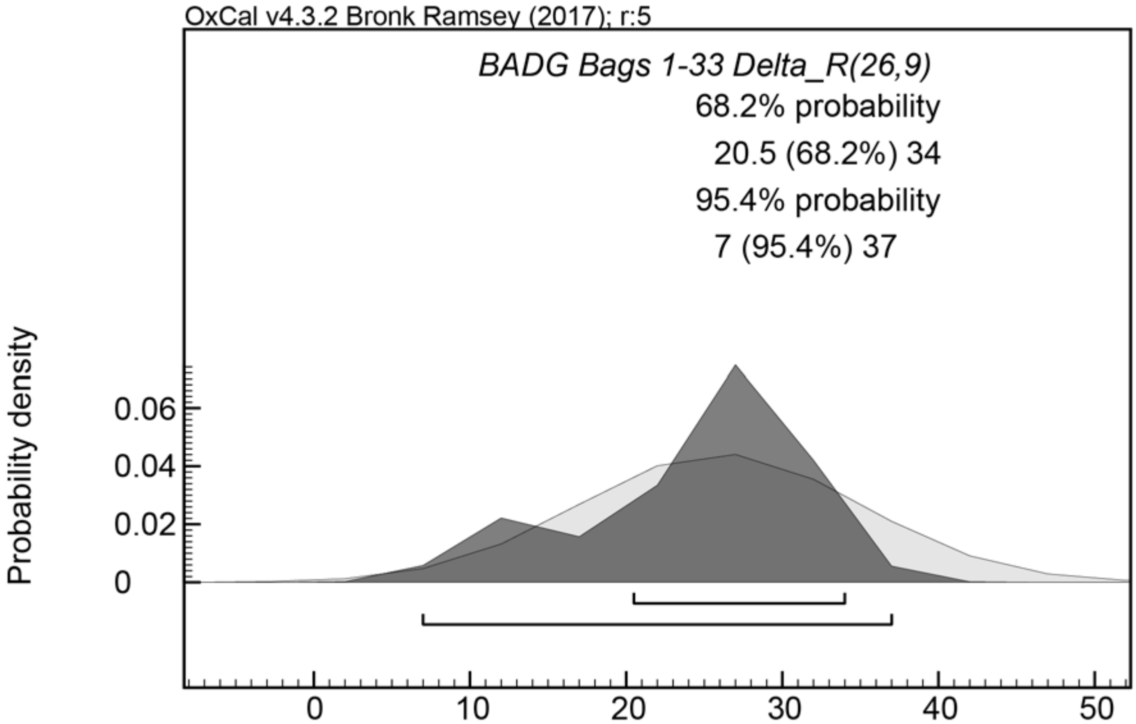

Fig. S15. The overall (average) offset between the BADG ^{14}C age ordered sequence as best placed versus the IntCal13 (17) curve via a Delta_R query in OxCal (19) with the prior value of 26±9 ^{14}C years (from Fig. S11) (thus the dataset in Table S6 changing the Delta_R value to 26,9). This assumed prior is shown by the light gray region. The calculated posterior density (the dark gray region) shows a good overlap, confirming the average offset range proposed (contrast with the lack of overlap with the neutral priors in Figs. S13 and S14).

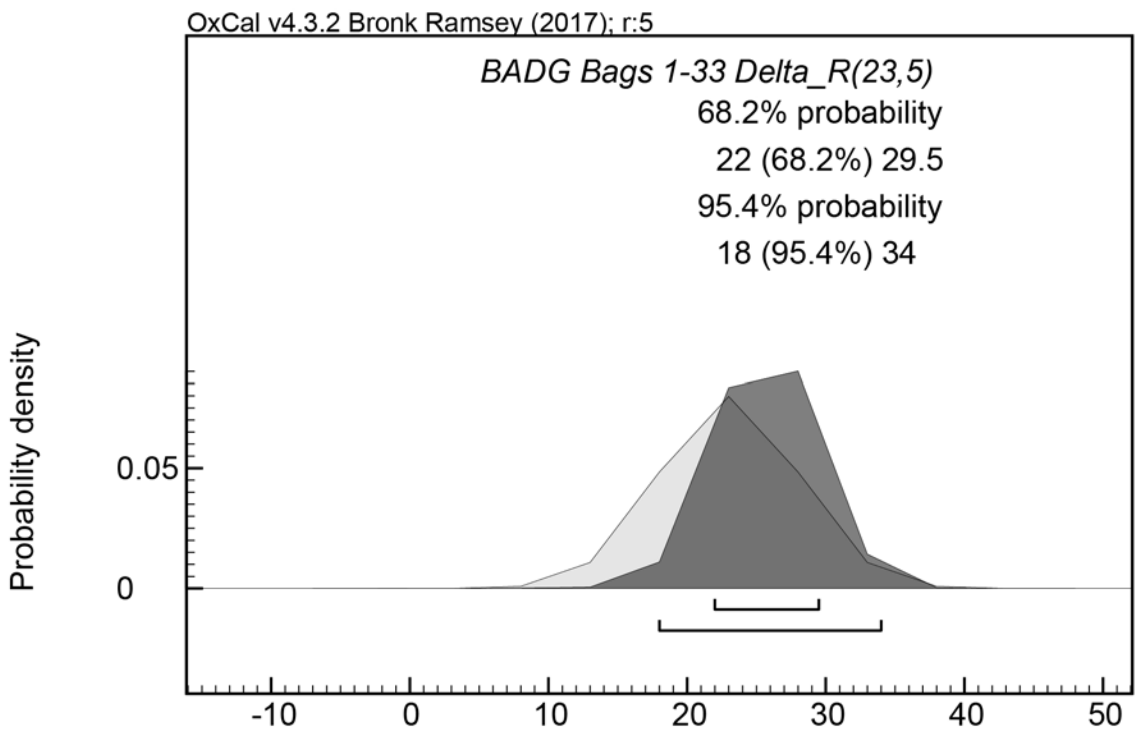

Fig. S16. As Fig. S15 but employing the prior value for the offset of 23±5 ^{14}C years from Fig. S14.

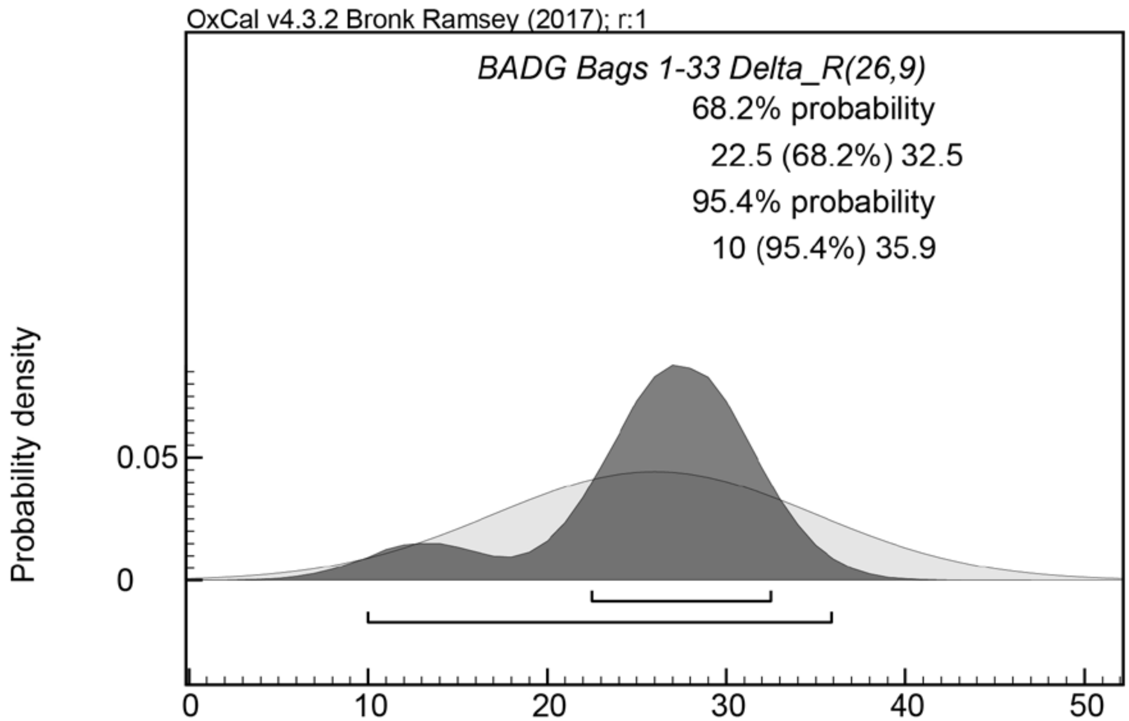

Fig. S17. As Fig. S15, but with curve resolution set at 1 year.

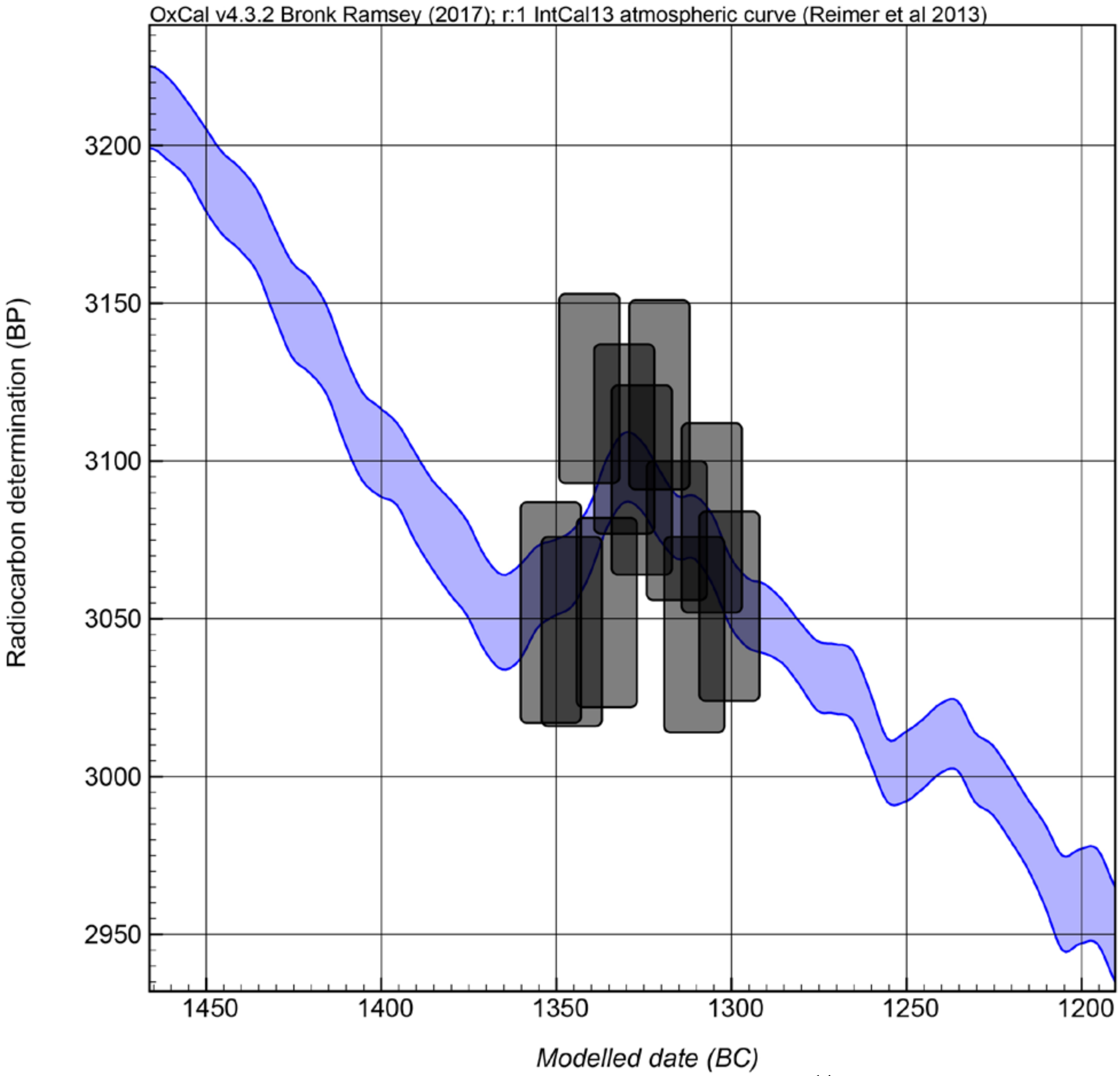

Fig. S18. The D_Sequence fit of the Oxford (OxA) data on a set of 12 ^{14}C dates on 11 known-age tree-ring samples of German Oak (25) against IntCal13 (17) employing OxCal (19) (two measurements on the same rings are combined (18)). Curve resolution set at 1 year. The boxes represent the 68.2% probability ranges in terms of both ^{14}C and calendar ranges. The IntCal13 curve is shown in blue as a 68.2% probability band. Amodel =118.8, Aoverall 122.3 well above the satisfactory threshold values of 60. All data include the known ages within the modelled most likely 68.2% hpd ranges.

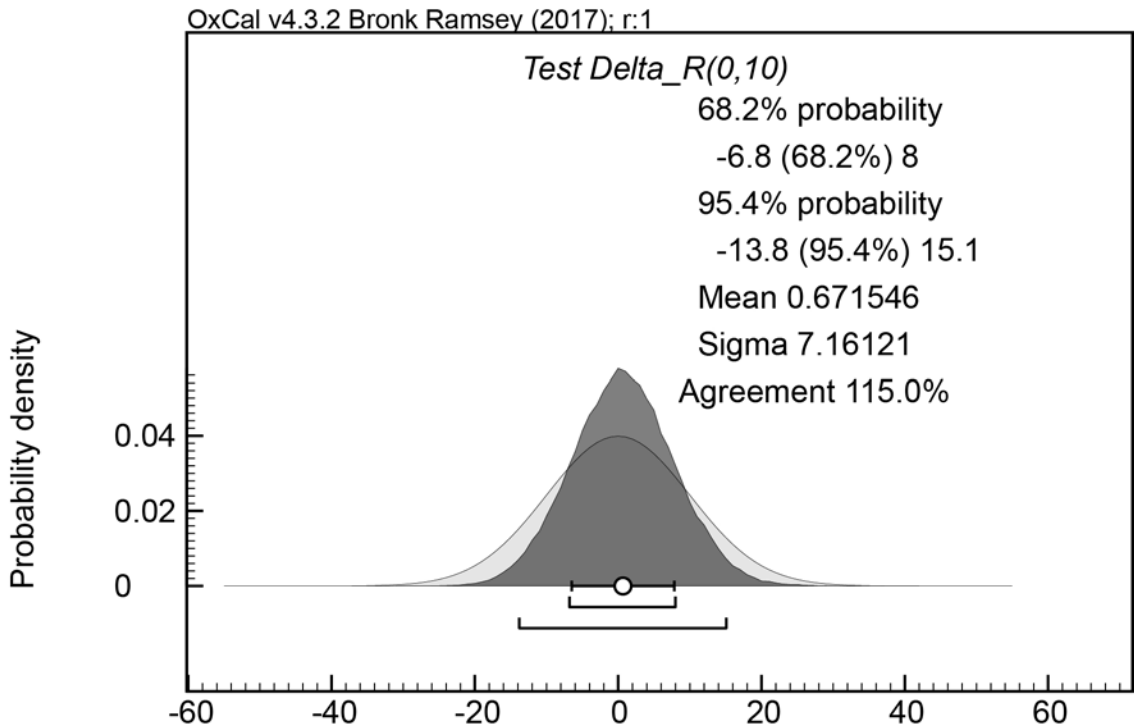

Fig. S19. The overall (average) offset (posterior density) between the OxA ^{14}C ages on German Oak (25) as best placed in Fig. S18 versus the IntCal13 (17) curve via a Delta_R query in OxCal (19) with a neutral prior of 0±10 ^{14}C years. There is a negligible (to approximately zero) offset of 0.7±7.2 ^{14}C years.

Fig. S20. Photos, taken in 2011, showing some examples of *Juniperus phoenicea* timbers in use in doors, doorways, roof/ceiling beams and other structural elements at Taybet Zaman.

Table S1. Tree-ring measurements in 1/1000ths (0.001) of a mm by year in Tucson (.rwl) format for each of the ten TZM samples employed in this study and as shown crossdated in Fig. S1: TZM1 (=file TZM012 below), TZM3 (=file TZM031 below), TZM4 (=file TZM041 below), TZM9 (=file TZM091 below), TZM12 (=file TZM121 below), TZM15 (=file TZM151 below), TZM16 (=file TZM161 below), TZM17 (=file TZM171 below), TZM23 (=file TZM231 below), TZM33&36 (=file TZM330 below).

```
TZM    1 Taybet Zaman                                           JUPH
TZM    2 Jordan     Juniperus phoenicea      ~1300M +3015 +3528     1610-1940
TZM    3 Katherine Seufer   Carol Griggs   Sturt Manning
TZM012  1742    26    39    35     3    38    53    10    36
TZM012  1750    16    21    35    16    32    18     3    26     6    16
TZM012  1760    27    12    25     2    22     6     3     2    17    13
TZM012  1770     7    34    11    28    39    26    31    43     2    45
TZM012  1780    30     7    15    10    16    13     2     2     6     2
TZM012  1790    21    24    10    11    10    21    22    42    33    45
TZM012  1800     4    64    50    91    84   125   133   178   170   175
TZM012  1810   123   118    68    55    60    70    85    53    83    70
TZM012  1820    75    91    98    66    90    81    84    30    62    45
TZM012  1830    49    52    91    68    60    81    76    61    62    65
TZM012  1840    34    23    36    51    43     7    15     2    11    51
TZM012  1850    23    44    38    46    17    46    31    47    31    35
TZM012  1860    63    55    50    69    69    36    56    48    78    60
TZM012  1870    43    30    44    25    31    39    49    35    66    46
TZM012  1880    82    41    41    31    60    69    85    73    49    58
TZM012  1890    55    65    54    56    39     3    57    30    22    12
TZM012  1900    29    60    52    45    49    48    33    60    88    21
TZM012  1910    55    69    37    44    47    73    52    45    64   999
TZM031  1765    55    40    48    72    35
TZM031  1770    79    96    69    26   113   117    60    52     9    24
TZM031  1780    51    77    49    55    57    59     3    19    32    59
TZM031  1790    68    36    14    42    83     8    10    43    37    66
TZM031  1800     9     7    58    34    45    62    30    38    19    75
TZM031  1810    52    43    32    20     4    14    10     9    15    63
TZM031  1820    51    19    55    58    40    44    67    30    33    85
TZM031  1830    99    46   122   121    90   138   284   123   101   181
TZM031  1840    82    47    49    90   121    32    66    45    27   122
TZM031  1850    99   235   139   131    26    79    70    86    40    76
TZM031  1860    80    85   124    72    58    31   136    64    93   124
TZM031  1870    40     3    26    11    54    54   102   110   116    74
TZM031  1880   135   119    95    45   164    93    99   121   122   215
TZM031  1890   161   130   103   106   123    16   174   157    94    82
TZM031  1900   168   188   135    99    33    98    70   138   198    96
TZM031  1910   108   159   103    91   999
TZM041  1719    37
TZM041  1720    44    45    63    33    25    38    27    42    28    21
TZM041  1730    35    24    56    32    33    28     2    15    11    13
TZM041  1740     7     8    13    50    29    11    38    24     1    18
TZM041  1750    25     7    28    14    20    40    19    43    29     7
TZM041  1760    23    21    20     2     2    41    27     2    91    20
TZM041  1770   117    86    53    14   113   130    95   106    38    35
TZM041  1780    71   124   157   120   103   117    12    22    25    54
TZM041  1790    56    30    13    51   121    23    17    44   104    69
TZM041  1800    70   114    58    44    66    76    55    38    23    19
TZM041  1810    33    21    17     6     4     9    15    42    39     1
```

TZM041	1820	12	46	51	72	54	59	54	4	73	159
TZM041	1830	193	160	267	316	129	291	227	77	65	105
TZM041	1840	96	50	66	85	114	24	57	36	27	76
TZM041	1850	65	135	168	143	26	168	148	73	51	50
TZM041	1860	59	82	99	105	72	25	100	79	74	66
TZM041	1870	9	3	25	28	60	52	138	64	90	55
TZM041	1880	59	70	51	31	54	57	53	60	22	51
TZM041	1890	42	55	29	18	29	2	36	39	27	19
TZM041	1900	46	70	48	47	40	42	34	36	30	23
TZM041	1910	30	20	20	999						
TZM091	1822	14	14	41	42	32	3	56	46		
TZM091	1830	58	34	60	68	62	113	91	64	65	113
TZM091	1840	83	34	56	71	123	45	95	60	47	124
TZM091	1850	142	192	234	111	31	195	174	125	84	78
TZM091	1860	88	71	149	125	118	57	127	127	132	166
TZM091	1870	27	7	61	56	80	163	347	158	157	87
TZM091	1880	131	104	96	94	145	122	161	105	42	87
TZM091	1890	94	170	133	127	147	14	134	129	79	73
TZM091	1900	81	203	85	139	74	117	129	136	162	71
TZM091	1910	135	231	999							
TZM121	1737	12	21	29							
TZM121	1740	40	45	17	21	30	26	44	40	7	29
TZM121	1750	83	22	58	62	18	21	29	23	23	3
TZM121	1760	10	15	43	30	23	17	11	10	19	2
TZM121	1770	12	7	10	5	103	67	81	51	25	49
TZM121	1780	105	192	93	84	90	90	12	16	43	19
TZM121	1790	60	48	30	75	123	46	44	46	57	69
TZM121	1800	138	113	64	79	7	87	4	9	3	13
TZM121	1810	5	23	21	8	14	8	4	24	40	45
TZM121	1820	56	77	98	75	98	159	103	14	35	60
TZM121	1830	54	79	141	223	140	266	270	92	106	106
TZM121	1840	65	25	18	22	44	17	27	31	11	44
TZM121	1850	49	85	99	63	55	104	92	110	93	97
TZM121	1860	63	120	97	120	67	31	48	15	50	50
TZM121	1870	54	11	45	17	94	40	58	32	69	33
TZM121	1880	68	70	89	79	162	144	87	107	39	68
TZM121	1890	84	92	79	78	94	64	226	115	94	84
TZM121	1900	83	124	110	100	79	101	79	115	143	68
TZM121	1910	93	104	66	96	54	42	33	39	63	34
TZM121	1920	29	15	999							
TZM151	1610	51	65	71	68	35	67	44	46	48	49
TZM151	1620	65	8	5	42	89	7	13	59	79	94
TZM151	1630	91	67	24	53	64	22	48	36	62	43
TZM151	1640	85	38	29	37	87	87	74	58	2	26
TZM151	1650	11	10	32	26	21	43	7	59	59	71
TZM151	1660	51	52	56	56	3	28	9	18	38	17
TZM151	1670	27	37	62	62	49	83	25	76	26	44
TZM151	1680	2	58	51	69	64	35	97	111	7	112
TZM151	1690	59	3	9	65	73	88	49	68	21	52
TZM151	1700	60	32	41	43	69	66	35	74	22	56
TZM151	1710	55	69	62	27	47	71	60	66	67	32
TZM151	1720	59	32	39	33	29	50	34	63	43	42
TZM151	1730	12	27	28	23	62	23	15	30	50	66
TZM151	1740	49	45	52	91	3	18	71	57	14	55
TZM151	1750	29	29	58	39	84	35	23	2	2	2
TZM151	1760	40	29	2	2	2	2	2	35	76	35
TZM151	1770	53	57	20	2	34	38	47	40	16	32

TZM151	1780	30	28	35	44	17	41	9	18	14	19
TZM151	1790	9	14	16	39	42	3	7	18	25	25
TZM151	1800	35	37	36	40	28	35	28	20	10	21
TZM151	1810	19	10	19	12	2	7	10	5	15	11
TZM151	1820	20	21	4	13	16	27	21	2	18	26
TZM151	1830	17	23	33	28	13	32	32	33	36	28
TZM151	1840	17	14	23	14	6	19	13	10	8	15
TZM151	1850	6	21	45	41	6	54	29	24	8	10
TZM151	1860	14	10	11	5	7	2	20	15	13	19
TZM151	1870	2	2	2	2	4	23	50	37	27	19
TZM151	1880	24	18	25	16	24	20	13	22	3	18
TZM151	1890	22	19	10	13	10	2	21	29	21	22
TZM151	1900	27	33	16	24	16	20	24	25	37	15
TZM151	1910	24	999								
TZM161	1638	25	40								
TZM161	1640	73	38	55	33	43	55	35	55	23	43
TZM161	1650	50	50	75	70	80	65	53	93	80	75
TZM161	1660	63	83	105	115	45	53	40	35	48	40
TZM161	1670	35	40	60	58	40	78	68	88	93	110
TZM161	1680	60	88	115	100	103	140	120	98	35	65
TZM161	1690	75	30	35	60	80	80	115	95	48	60
TZM161	1700	58	68	45	2	78	75	68	83	48	45
TZM161	1710	43	43	40	33	38	40	58	53	85	70
TZM161	1720	90	45	55	63	58	60	55	50	45	45
TZM161	1730	23	50	40	5	25	35	23	30	23	30
TZM161	1740	48	53	65	50	75	18	58	65	38	73
TZM161	1750	45	55	58	70	63	55	63	80	68	63
TZM161	1760	90	60	53	25	55	40	15	15	35	35
TZM161	1770	25	45	40	55	78	58	60	95	15	43
TZM161	1780	55	10	30	28	20	33	2	20	15	13
TZM161	1790	30	38	13	30	43	30	25	35	30	33
TZM161	1800	5	30	25	33	23	20	15	10	15	13
TZM161	1810	13	999								
TZM171	1815	18	18	25	22	25					
TZM171	1820	34	26	31	25	17	18	10	6	9	13
TZM171	1830	20	29	40	32	37	30	34	18	54	127
TZM171	1840	139	112	76	116	140	48	50	51	86	106
TZM171	1850	107	106	113	123	58	93	120	93	54	79
TZM171	1860	95	84	99	82	101	77	100	72	87	83
TZM171	1870	85	33	59	36	47	85	84	104	115	94
TZM171	1880	103	156	171	134	139	171	185	150	152	182
TZM171	1890	139	181	149	139	97	80	134	120	94	108
TZM171	1900	161	229	162	127	170	109	113	143	127	78
TZM171	1910	97	118	140	159	130	182	143	181	171	999
TZM231	1754	10	20	20	38	30	28				
TZM231	1760	43	40	38	35	55	43	38	35	45	60
TZM231	1770	45	55	35	40	53	50	43	43	7	35
TZM231	1780	48	23	25	20	23	33	2	20	50	40
TZM231	1790	43	35	13	15	35	40	43	70	83	83
TZM231	1800	28	60	50	100	68	75	53	53	45	35
TZM231	1810	35	33	15	28	18	30	40	25	128	75
TZM231	1820	80	53	68	48	50	55	65	20	40	13
TZM231	1830	25	28	50	63	50	48	55	50	55	50
TZM231	1840	68	30	43	48	95	20	55	30	23	38
TZM231	1850	35	35	63	135	83	130	103	85	73	73
TZM231	1860	75	73	65	75	65	50	68	43	58	65
TZM231	1870	53	23	15	7	5	30	45	28	28	23

TZM231	1880	53	43	70	55	65	88	138	135	128	120
TZM231	1890	105	105	150	165	188	105	153	115	123	75
TZM231	1900	128	153	145	125	100	108	98	100	118	70
TZM231	1910	80	73	98	80	100	125	130	120	143	83
TZM231	1920	43	73	65	53	70	50	70	28	75	68
TZM231	1930	95	60	55	53	58	58	10	55	70	108
TZM231	1940	93	999								
TZM330	1799	55									
TZM330	1800	31	30	35	13	26	41	50	46	59	64
TZM330	1810	31	46	22	29	32	34	50	66	52	38
TZM330	1820	49	33	60	39	29	38	43	17	50	51
TZM330	1830	42	26	43	36	34	39	28	19	29	32
TZM330	1840	41	30	33	42	39	17	30	26	23	33
TZM330	1850	31	60	78	76	37	41	60	71	54	62
TZM330	1860	51	47	20	24	27	26	47	27	48	49
TZM330	1870	38	17	14	14	15	30	44	33	54	44
TZM330	1880	61	55	68	57	68	82	85	60	62	61
TZM330	1890	49	42	30	34	37	10	50	28	29	26
TZM330	1900	28	21	47	63	81	76	75	86	109	58
TZM330	1910	75	68	54	43	39	35	27	28	53	52
TZM330	1920	38	84	58	49	52	52	51	16	36	24
TZM330	1930	26	6	9	8	12	999				

Table S2. Dendrochronologically dated TZM *Juniperus phoenicea* tree-ring samples (Cornell TZM numbers) and their corresponding ^{14}C dates from Oxford and Arizona. The OxA-X-2646-40 and OxA-X-2646-46 results followed non-routine chemistry; instead of employing a soxhlet extraction, test tubes and heating blocks were used. Since no significance difference in results is evident we use these dates. OxA-32832 is clearly too old and an outlier. There is no obvious explanation from laboratory data. This result is not employed in the analyses in our paper. AA-103300 is very clearly far too old and a massive outlier. There is no explanation from laboratory data. This result is not employed in the analyses in our paper. Where two or three OxA dates were run on the identical sample, a weighted average has been calculated (17) and this is used in the subsequent analysis (such as Figs. 2, 3, S3). The exception is the AD1818-1822 sample where there are four data and OxA-29735 is an outlier and is not included in the weighted average value for this sample. The codes for the Oxford pretreatment regime (14) are: UW = ABA+bleach pretreatment, UA = α-cellulose pretreatment, * = solvent extraction (acetone then water for OxA- ≤32830; 1:1 (v/v) chloroform/ethanol, then ethanol, then water for OxA- ≥34703). Quoted $\delta^{13}C$ values are independent stable isotope mass spectrometer measurements per mil relative to VPDB.

OxA-	Tree TZM-	Start Year AD	End Year AD	^{14}C Age	SD	$\delta^{13}C$	Weighted average ^{14}C Age	SD	OxA Pretreatment Regime
Oxford (OxA), Taybet Zaman (TZM)									
32744	15	1610	1614	380	24	-17.4			UA*
32745	15	1615	1619	404	24	-17.8			UA*
32746	15	1620	1624	275	26	-18.1			UA*
32747	15	1625	1629	408	23	-18.2			UA*
X-2646-40	15	1630	1634	322	23	-18.2			UA*
32748	15	1630	1634	307	23	-18.6	315	17	UA*
32574	15	1635	1639	266	26	-18.2			UA*
32575	15	1640	1644	274	24	-17.9			UA*
32576	15	1645	1649	260	24	-18.1			UA*
32577	15	1650	1654	273	25	-18.0			UA*
32578	15	1655	1659	238	24	-18.3			UA*
32579	15	1660	1664	200	25	-17.7			UA*
32580	15	1665	1669	234	24	-17.7			UA*
32581	15	1670	1674	214	25	-18.1			UA*
32749	15	1675	1679	206	24	-18.6			UA*
32582	15	1680	1684	146	25	-18.3			UA*
32583	15	1685	1689	157	24	-18.3			UA*
32584	15	1690	1694	171	24	-17.4			UA*
32750	15	1695	1699	129	23	-17.4			UA*
32831	15	1700	1704	147	24	-17.6			UA*
32751	15	1705	1709	120	23	-17.5			UA*
32752	15	1710	1714	143	24	-18.1			UA*
X-2646-46	15	1715	1719	126	23	-17.3			UA*

32753	15	1715	1719	141	24	-17.3	133	17	UA*
32754	15	1720	1724	122	23	-16.9			UA*
29718	4	1723	1727	119	22	-21.5			UW
32755	15	1725	1729	177	23	-17.0			UA*
29719	4	1728	1732	141	22	-21.1			UW
29720	4	1733	1737	152	22	-20.8			UW
32756	15	1735	1739	191	23	-17.1			UA*
29721	4	1738	1742	122	23	-19.7			UW
32828	4	1738	1742	175	24	-18.1	148	17	UA*
32757	15	1740	1744	184	23	-17.2			UA*
29722	4	1743	1747	132	21	-20.2			UW
32832	15	1745	1749	382	24	-17.1			UA*
29924	4	1748	1752	228	22	-20.2			UW
32758	15	1750	1754	159	23	-17.9			UA*
29723	4	1753	1757	199	22	-20.1			UW
29724	4	1758	1762	177	22	-20.4			UW
29725	4	1763	1767	129	22	-20.1			UW
29726	4	1768	1772	198	23	-19.9			UW
32829	4	1768	1772	253	24	-18.3	224	17	UA*
29727	4	1773	1777	136	21	-20.2			UW
29728	4	1773	1777	160	22	-20.1	147	16	UW
29729	4	1778	1782	221	21	-19.8			UW
29730	4	1783	1787	205	22	-20.6			UW
29731	4	1788	1792	231	23	-19.2			UW
29732	4	1793	1797	208	23	-19.3			UW
29733	4	1798	1802	203	21	-20.3			UW
29734	4	1803	1817	140	22	-16.9			UW
29735	4	1818	1822	57	22	-19			UW
32830	4	1818	1822	124	23	-18.7			UA*
35659	4	1818	1822	111	25	-19.0			UW*
36014	4	1818	1822	112	23	-18.6	116	14	UA*
29389	3	1823	1827	132	25	-20.0			UW
29390	3	1828	1832	119	25	-19.9			UW
29445	3	1833	1837	92	25	-21.2			UW
32825	3	1833	1837	118	26	-19.4	105	19	UA*
29446	3	1838	1842	142	25	-20.7			UW
29447	3	1843	1847	163	25	-20.2			UW
29717	3	1848	1852	110	21	-20.3			UW
32826	3	1848	1852	161	24	-18.8	132	16	UA*
29448	3	1853	1857	126	24	-21.1			UW
29449	3	1858	1862	156	23	-19.9			UW
29450	3	1863	1867	141	24	-20.5			UW
29867	3	1868	1872	111	24	-20.1			UW

29530	3	1873	1877	150	23	-20.7			UW
29531	3	1878	1882	87	25	-20.2			UW
32827	3	1878	1882	103	23	-18.3	96	17	UA*
29532	3	1883	1887	181	24	-20.7			UW
34703	3	1883	1887	158	23	-19.2	169	17	UA*
29533	3	1888	1892	131	24	-21.0			UW
35658	3	1888	1892	127	23	-20.3			UW*
36013	3	1888	1892	131	24	-19.4	130	14	UA*
29534	3	1893	1897	162	22	-20.8			UW
34705	3	1893	1897	114	23	-19.4	139	16	UA*
29535	3	1898	1902	139	23	-20.8			UW
34706	3	1898	1902	146	22	-19.5	143	16	UA*
29536	3	1903	1907	133	24	-20.7			UW
34707	3	1903	1907	98	24	-19.4	116	17	UA*
29537	3	1908	1912	105	24	-19.5			UW
34708	3	1908	1912	148	23	-19.4	128	17	UA*
AA-									
Arizona (AA), Taybet Zaman (TZM)									
105490	15	1610	1614	380	25	-17.7			
105491	15	1615	1619	357	25	-20.5			
105492	15	1620	1624	335	25	-20.4			
105493	15	1625	1629	376	30	-21.7			
105494	15	1630	1634	359	25	-18.6			
105489	15	1635	1639	281	25	-20.3			
105488	15	1640	1644	258	30	-18.9			
105487	15	1645	1649	229	30	-19.1			
105486	15	1650	1654	241	26	-20.8			
105485	15	1655	1659	233	29	-20.8			
105484	15	1660	1664	207	26	-19.7			
105483	15	1665	1669	196	26	-18.7			
105482	15	1670	1674	151	21	-21			
105481	15	1675	1679	132	27	-22			
105480	15	1680	1684	123	27	-21			
105479	15	1685	1689	148	27	-19.6			
105478	15	1690	1694	142	27	-19.4			
105477	15	1695	1699	114	27	-18.8			
105476	15	1700	1704	97	29	-19			
105475	15	1705	1709	146	30	-17.2			
105474	15	1710	1714	91	22	-18.8			
105473	15	1715	1719	143	30	-21			
105472	15	1720	1724	165	21	-20.7			
105471	15	1725	1729	194	23	-20			

105470	4	1730	1734	185	23	-20.1			
105469	15	1735	1739	124	41	-17.5			
105468	15	1740	1744	203	38	-17.5			
105467	15	1745	1749	186	31	-18.5			
105466	15	1750	1754	171	41	-18.1			
103288	3	1823	1827	106	29	-22.5			
103289	3	1828	1832	82	33	-20.3			
103290	3	1833	1837	112	29	-22.2			
103291	3	1838	1842	168	32	-20.9			
103292	3	1843	1847	112	30	-19.5			
103293	3	1848	1852	148	31	-21.6			
103294	3	1853	1857	130	33	-22.7			
103295	3	1858	1862	106	29	-20.3			
103296	3	1863	1867	175	32	-20.1			
103297	3	1868	1872	179	33	-20.3			
103298	3	1873	1877	146	33	-22.3			
103299	3	1878	1882	166	34	-20.8			
103300	3	1883	1887	1081	22	-21.6			
103301	3	1888	1892	179	33	-20.9			
103302	3	1893	1897	84	38	-21.3			
103303	3	1898	1902	130	33	-20.9			
103304	3	1903	1907	130	33	-21.3			
103305	3	1908	1912	162	33	-20.3			

Table S3. The ordered sequence of BADG *Juniperus phoenicea* tree-ring samples and their corresponding ^{14}C dates from Oxford and Arizona. In total, the dataset comprises Bag 1, oldest, to Bag 50, most recent, but, as discussed in the SI Text, only the ordered sequence from Bag 1 to Bag 33 was employed for the analysis. The data in the gray-shaded cells were *not* employed. Where there were 32XXX series OxA dates (*OxA2* column in the table) we used these data instead (Bag 29) as these data were re-run samples using full α-cellulose (and consistently returned older ^{14}C ages). PB = post-bomb ^{14}C age. Three AA dates were reported initially as post-bomb and then subsequently re-run (as α-cellulose) and returned more plausible ^{14}C ages. Quoted $\delta^{13}C$ values are independent stable isotope mass spectrometer measurements per mil relative to VPDB (no data are available where not listed). Where the AA and OxA data could be combined (18) a weighted average (Av) is given (and used in Figs. S8-S10).

Bag No.	AA-	$\delta^{13}C$	^{14}C	SD	*OxA1* OxA-	$\delta^{13}C$	^{14}C	SD	*OxA2* OxA-	$\delta^{13}C$	^{14}C	SD	Av	SD
1	103219	-20.3	213	25	29538	-19.6	289	23					N/A	N/A
2	103220	-21.3	187	16	29539	-20.0	190	24					188	14
3	103221	-21.7	170	21	29540	-19.7	195	23					181	16
4	103222	-21.1	154	33	29451	-20.2	184	23					174	19
5	103223	-21.6	166	21	29391	-20.1	162	24					164	16
6	103224		162	16	29452	-19.8	161	23					162	14
7	103225	-20.5	139	22	29392	-19.9	149	24					144	17
8	103226		121	16	29393	-19.8	197	25					N/A	N/A
9	103227	-21.4	144	22	29394	-20.1	133	25					139	17
10	103228	-21.1	102	22	29395	-20.7	152	25					124	17
11	103229	-22.2	121	24	29420	-20.6	163	21					145	16
12	103230	-21.6	130	16	29421	-20.7	149	22					125	12
12					29422	-20.2	96	21						
13	103231	-21.9	179	25	29423	-19.7	188	21					184	17
14	103232	-22.3	203	21	29424	-20.1	242	20					224	15
15	103233	-22.3	195	25	29425	-20.0	203	21					200	17
16	103234	-20.7	175	23	29426	-20.4	220	21					200	16
17	103235	-21.5	203	21	29427	-19.8	189	20					196	15
18					29488	-19.8	189	22						
19	103237	-20.7	198	21	29489	-19.6	181	22					190	16
20	103238	-21.6	195	16	29490	-19.9	176	22					188	13
21					29453	-20.0	222	25						
22	103240	-20.9	222	21	29454	-19.6	202	24					213	16
23	103241	-20.7	290	22	29455	-19.7	234	24					265	17
24	103242	-20.3	180	24	29456	-19.8	169	24					175	17
25	103243	-21.9	187	16	29457	-20.2	153	24					177	14
26	103244	-21.9	179	16	29458	-19.5	204	25					186	14
27	103245	-20.8	146	16	29823	-19.2	107	22					133	13
28	103246	-20.6	128	22	29459	-18.8	125	23					127	16
29					29616	-19.4	67	23	32071	-18.4	89	24	79	17

29									32119	-18.5	69	24		
30	103248	-20.8	130	22	29460	-19.3	66	23	32735	-18.8	117	25	124	17
31					29461	-19.7	140	23	--	--	--	--	140	23
32	103250	-20.7	162	16	29462	-19.1	162	23	--	--	--	--	152	12
32					29463	-19.0	121	23	--	--	--	--		
33	103251	-20.1	138	16	29464	-19.0	120	23	--	--	--	--	132	14
34	103252	-21.3	179	16	29617	-19.1	57	24	32736	-18.2	82	24		
35	103253	-21.3	113	16	29824	-18.7	PB		--	--	--	--		
36	103254	-20.4	PB		29618	-19.1	50	23	32737	-18.0	131	24		
36	103254	-20.4	138	25										
37	103255		154	16	29825	-19.2	PB		--	--	--	--		
38	103256		146	16	29541	-19.1	62	23	32738	-18.1	124	24		
39	103257	-20.4	187	22	29542	-19.2	100	24	--	--	--	--		
40	103258		162	25	29619	-19.4	24	23	32739	-18.4	114	24		
41	103259	-21	PB		29620	-19.7	66	24	32740	-18.7	96	24		
41	103259	-21	54	19										
42	103260		83	20	29621	-19.9	80	23	32741	-19.0	149	23		
43	103261		83	16	29622	-19.7	71	23	32742	-18.8	128	23		
44	103262	-21.1	5	31	29623	-19.7	40	23	32743	-18.5	158	23		
45	103263	-21.8	PB		29624	-19.8	PB		32035	-18.2	182	23		
45		-21.8	151	16					32036	-18.1	66	22		
46	103264		138	16	29625	-19.8	103	24	--	--				
47					29626	-18.9	156	23	--	--				
48	103266	-20.8	185	22	29627	-19.2	120	23	--	--				
49	103267	-21.8	130	22	29628	-20.0	PB		32037	-18.3	179	22		
49									32038	-18.3	PB			
50					29629	-19.4	74	23	34709	-18.9	PB			

Table S4. TZM ^{14}C data, combining (where possible) the available AA and OxA data (Fig. S3), compared to the contemporary mean IntCal13 value (17) and tested for significant (95%) difference (18). Linear interpolation is applied to the IntCal13 dataset to achieve the relevant annual year values when between the 5-year IntCal13 values.

Year AD	TZM ^{14}C	TZM SD	IntCal13 ^{14}C	IntCal13 SD	T value	TZM Older (71% data)
1612	380	18	357.6	7.6	1.3	X
1617	382	18	346.0	7.0	3.5	X
1622	306	19	333.2	7.0	1.8	
1627	396	19	330.4	7.4	10.4	X
1632	328	14	319.2	7.6	0.3	X
1637	274	19	303.2	7.0	2.1	
1642	268	19	288.6	7.0	1.0	
1647	248	19	264.6	7.0	0.7	
1652	258	19	246.8	7.0	0.3	X
1657	236	19	236.6	7.0	0.0	
1662	203	19	225.8	7.0	1.3	
1667	217	18	201.4	7.4	0.6	X
1672	177	17	179.0	7.6	0.0	
1677	174	18	172.4	7.4	0.0	X
1682	135	19	156.6	7.6	1.1	
1687	153	18	137.8	6.6	0.6	X
1692	158	18	127.0	5.6	2.7	X
1697	123	18	112.0	5.4	0.3	X
1702	127	19	103.8	6.0	1.4	X
1707	130	19	101.8	6.0	2.0	X
1712	115	17	95.4	6.4	1.2	X
1717	135	15	97.8	6.6	5.2	X
1722	146	16	108.2	6.0	4.9	X
1725	119	22	113.9	6.0	0.0	X
1727	186	17	122.6	6.8	12.1	X
1730	141	22	136.5	8.0	0.0	X
1732	185	23	143.0	8.0	3.0	X
1735	152	22	152.0	8.0	0.0	
1737	175	21	158.0	7.6	0.6	X
1740	148	17	165.9	7.0	0.9	
1742	189	20	165.4	7.0	1.2	X
1745	132	21	163.2	7.0	2.0	
1747	186	31	163.0	7.0	0.5	X
1750	228	22	162.9	7.0	8.0	X
1752	162	21	162.2	7.0	0.0	
1755	199	22	160.8	7.0	2.8	X
1760	177	22	156.2	7.0	0.8	X

1765	129	22	171.3	8.0	3.3	
1770	224	17	175.4	8.0	6.7	X
1775	147	16	169.3	7.0	1.6	
1780	221	21	185.7	7.0	2.6	X
1785	205	22	213.7	8.0	0.1	
1790	231	23	218.5	8.0	0.3	X
1795	208	23	210.3	8.0	0.0	
1800	203	21	171.2	7.0	2.1	X
1810	140	22	132.0	8.0	0.1	X
1820	116	14	102.4	6.0	0.8	X
1825	121	19	102.6	7.0	0.8	X
1830	106	20	96.0	7.0	0.2	X
1835	107	16	112.7	8.0	0.1	
1840	152	20	121.4	8.0	2.0	X
1845	142	20	114.3	8.0	1.7	X
1850	135	15	114.3	9.0	1.4	X
1855	127	20	121.6	8.0	0.1	X
1860	137	19	119.2	6.0	0.8	X
1865	153	20	122.6	6.0	2.1	X
1870	135	20	114.4	6.0	1.0	
1875	149	19	118.5	7.0	2.3	
1880	110	16	104.3	7.0	0.1	X
1885	169	17	102.0	7.0	13.4	X
1890	137	13	97.6	7.0	7.1	X
1895	131	15	78.3	7.0	10.2	X
1900	140	15	71.4	7.0	17.3	X
1905	119	16	83.1	7.0	4.2	X
1910	135	15	98.8	7.0	4.8	X

Table S5. OxCal (19) runfile for the OxA Delta_R plot shown in Fig. 2C. This is given as an example for the other similar plots in Fig. 2C, Fig. 3C, SI Appendix Fig. 4A which are similar *but* employ the relevant data from Table S2 and against the stated calibration dataset. IntCal13 (17) is the current default calibration dataset in OxCal. To employ SHCal13 (50), as reported in Fig. 3A, this must be specified adding the code under Options reading: Curve="ShCal13.14c";

```
Options()
 {
  Resolution=1;
 };
 Plot()
 {
  Delta_R("OxA Jordan Juniper", 0, 20);
  D_Sequence ()
  {
   R_Date("OxA 32744 1612",380,24);
   Gap(5);
   R_Date("OxA 32745 1617",404,24);
   Gap(5);
   R_Date("OxA 32746 1622",275,26);
   Gap(5);
   R_Date("OxA 32747 1627",408,23);
   Gap(5);
   R_Combine ("1632")
   {
    R_Date("OxA 32748 1632",307,23);
    R_Date("OxAX-2646-40 1632",322,23);
   };
   Gap(5);
   R_Date("OxA 32574 1637",266,26);
   Gap(5);
   R_Date("OxA 32575 1642",274,24);
   Gap(5);
   R_Date("OxA 32576 1647",260,24);
   Gap(5);
   R_Date("OxA 32577 1652",273,25);
   Gap(5);
   R_Date("OxA 32578 1657",238,24);
   Gap(5);
   R_Date("OxA 32579 1662",200,25);
   Gap(5);
   R_Date("OxA 32580 1667",234,24);
   Gap(5);
   R_Date("OxA 32581 1672",214,25);
   Gap(5);
   R_Date("OxA 32749 1677",206,24);
   Gap(5);
   R_Date("OxA 32582 1682",146,25);
   Gap(5);
   R_Date("OxA 32583 1687",157,24);
   Gap(5);
   R_Date("OxA 32584 1692",171,24);
   Gap(5);
```

```
R_Date("OxA 32750 1697",129,23);
Gap(5);
R_Date("OxA 32831 1702",147,24);
Gap(5);
R_Date("OxA 32751 1707",120,23);
Gap(5);
R_Date("OxA 32752 1712",143,24);
Gap(5);
R_Combine ("1717")
{
 R_Date("OxA32753 1717",141,24);
 R_Date("OxAX-2646-46 1717",126,23);
};
Gap(5);
R_Date("OxA 32754 1722",122,23);
Gap(3);
R_Date("OxA 29718 1725",119,22);
Gap(2);
R_Date("OxA 32755 1727",177,23);
Gap(3);
R_Date("OxA 29719 1730",141,22);
Gap(5);
R_Date("OxA 29720 1735",152,22);
Gap(2);
R_Date("OxA 32756 1737",191,23);
Gap(3);
R_Combine ("1740")
{
 R_Date("OxA29721 1740",122,23);
 R_Date("OxA32828 1740",175,24);
};
Gap(2);
R_Date("OxA 32757 1742",184,23);
Gap(3);
R_Date("OxA 29722 1745",132,21);
Gap(5);
R_Date("OxA 29924 1750",228,22);
Gap(2);
R_Date("OxA 32758 1752",159,23);
Gap(3);
R_Date("OxA 29723 1755",199,22);
Gap(5);
R_Date("OxA 29724 1760",177,22);
Gap(5);
R_Date("OxA 29725 1765",129,22);
Gap(5);
R_Combine ("1770")
{
 R_Date("OxA29726 1770",198,23);
 R_Date("OxA32829 1770",253,24);
};
Gap (5);
R_Combine ("1775")
{
 R_Date("OxA29727 1775",136,21);
 R_Date("OxA29728 1775",160,22);
```

```
};
Gap (5);
R_Date("OxA 29729 1780",221,21);
Gap(5);
R_Date("OxA 29730 1785",205,22);
Gap(5);
R_Date("OxA 29731 1790",231,23);
Gap(5);
R_Date("OxA 29732 1795",208,23);
Gap(5);
R_Date("OxA 29733 1800",203,21);
Gap(10);
R_Date("OxA 29734 1810",140,22);
Gap(10);
R_Combine ("1820")
{
 R_Date("OxA32830 1820",124,23);
 R_Date("OxA 35659 1820",111,25);
 R_Date("OxA 36014 1820",112,23);
};
Gap(5);
R_Date("OxA 29389 1825",132,25);
Gap(5);
R_Date("OxA 29390 1830",119,25);
Gap(5);
R_Combine ("1835")
{
 R_Date("OxA29445 1835",92 ,25);
 R_Date("OxA32825 1835",118,26);
};
Gap(5);
R_Date("OxA 29446 1840",142,25);
Gap(5);
R_Date("OxA 29447 1845",163,25);
Gap(5);
R_Combine ("1850")
{
 R_Date("OxA29717 1850",110,21);
 R_Date("OxA32826 1850",161,24);
};
Gap(5);
R_Date("OxA 29448 1855",126,24);
Gap(  5);
R_Date("OxA 29449 1860",156,23);
Gap(  5);
R_Date("OxA 29450 1865",141,24);
Gap(  5);
R_Date("OxA 29867 1870",111,24);
Gap(  5);
R_Date("OxA 29530 1875",150,23);
Gap(  5);
R_combine ("1880")
{
 R_Date("OxA29531 1880",87,25);
 R_Date("OxA32827 1880",103,23);
};
```

```
  Gap(5);
  R_Combine ("1885")
  {
   R_Date("OxA29532 1885",181,24);
   R_Date("OxA34703 1885",158,23);
  };
  Gap(5);
  R_Combine ("1890")
  {
   R_Date("OxA29533 1890",131,24);
   R_Date("OxA 35658 1890",127,23);
   R_Date("OxA 36013 1890",131,24);
  };
  Gap(5);
  R_Combine ("1895")
  {
   R_Date("OxA29534 1895",162,22);
   R_Date("OxA34705 1895",114,23);
  };
  Gap(5);
  R_Combine ("1900")
  {
   R_Date("OxA29535 1900",139,23);
   R_Date("OxA34706 1900",146,22);
  };
  Gap(5);
  R_Combine ("1905")
  {
   R_Date("OxA29536 1905",133,24);
   R_Date("OxA34707 1905",98 ,24);
  };
  Gap(5);
  R_Combine ("1910")
  {
   R_Date("OxA29537 1910",105,24);
   R_Date("OxA34708 1910",148,23);
  };
 };
};
```

Table S6. OxCal (19) runfile for the BADG ordered sequence reported in Figs. S8, S11. Note for the data reported in Figs. S9 and S10 the lines of code below reading “Gap (5,2);” were replaced with “Gap (5,3);” and “Gap (5,4);” respectively.

```
Options()
 {
  Resolution=5;
 };
 Plot()
 {
  Delta_R ("BADG Bags 1-33",0,20);
  Sequence ("BADG Bags 1-33")
  {
   Boundary ("Start");
   Phase ("Bag 1")
   {
    R_Date("Bag 1 OxA-29538",289,23);
    R_Date("Bag 1 AA103219",213,25);
   };
   Gap (5,2);
   R_Combine ("Bag 2")
   {
    R_Date("OxA-29539",190,24);
    R_Date("AA103220",187,16);
   };
   Gap (5,2);
   R_Combine ("Bag 3")
   {
    R_Date("OxA-29540",195,23);
    R_Date("AA103221",170,21);
   };
   Gap (5,2);
   R_Combine ("Bag 4")
   {
    R_Date("OxA-29451",184,23);
    R_Date("AA103222",154,33);
   };
   Gap (5,2);
   R_Combine ("Bag 5")
   {
    R_Date("OxA-29391",162,24);
    R_Date("AA103223",166,21);
   };
   Gap (5,2);
   R_Combine ("Bag 6")
   {
    R_Date("OxA-29452",161,23);
    R_Date("AA103224",162,16);
   };
   Gap (5,2);
   R_Combine ("Bag 7")
   {
    R_Date("OxA-29392",149,24);
    R_Date("AA103225",139,22);
   };
```

```
Gap (5,2);
Phase ("Bag 8")
{
 R_Date("Bag 8 OxA-29393",197,25);
 R_Date("Bag 8 AA103226",121,16);
};
Gap (5,2);
R_Combine ("Bag 9")
{
 R_Date("OxA-29394",133,25);
 R_Date("AA103227",144,22);
};
Gap (5,2);
R_Combine ("Bag 10")
{
 R_Date("OxA-29395",152,25);
 R_Date("AA103228",102,22);
};
Gap (5,2);
R_Combine ("Bag 11")
{
 R_Date("OxA-29420",163,21);
 R_Date("AA103229",121,24);
};
Gap (5,2);
R_Combine ("Bag 12")
{
 R_Date("OxA-29421",149,22);
 R_Date("AA103230",130,16);
 R_Date("OxA-29422",96,21);
};
Gap (5,2);
R_Combine ("Bag 13")
{
 R_Date("OxA-29423",188,21);
 R_Date("AA103231",179,25);
};
Gap (5,2);
R_Combine ("Bag 14")
{
 R_Date("OxA-29424",242,20);
 R_Date("AA103232",203,21);
};
Gap (5,2);
R_Combine ("Bag 15")
{
 R_Date("OxA-29425",203,21);
 R_Date("AA103233",195,25);
};
Gap (5,2);
R_Combine ("Bag 16")
{
 R_Date("OxA-29426",220,21);
 R_Date("AA103234",175,23);
};
Gap (5,2);
```

```
R_Combine ("Bag 17")
{
 R_Date("OxA-29427",189,20);
 R_Date("AA103235", 203,21);
};
Gap (5,2);
R_Date ("Bag 18 OxA-29488",189,22);
Gap (5,2);
R_Combine ("Bag 19")
{
 R_Date("OxA-29489",181,22);
 R_Date("AA103237",198,21);
};
Gap (5,2);
R_Combine ("Bag 20")
{
 R_Date("OxA-29490",176,22);
 R_Date("AA103238",195,16);
};
Gap (5,2);
R_Date ("Bag 21 OxA-29453",222,25);
Gap (5,2);
R_Combine ("Bag 22")
{
 R_Date("OxA-29454",202,24);
 R_Date("AA103240",222,21);
};
Gap (5,2);
R_Combine ("Bag 23")
{
 R_Date("OxA-29455",234,24);
 R_Date("AA103241", 290,22);
};
Gap (5,2);
R_Combine ("Bag 24")
{
 R_Date("OxA-29456",169,24);
 R_Date("AA103242",180,24);
};
Gap (5,2);
R_Combine ("Bag 25")
{
 R_Date("OxA-29457",153,24);
 R_Date("AA103243",187,16);
};
Gap (5,2);
R_Combine ("Bag 26")
{
 R_Date("OxA-29458",204,25);
 R_Date("AA103244",179,16);
};
Gap (5,2);
R_Combine ("Bag 27")
{
 R_Date("OxA-29823",107,22);
 R_Date("AA103245", 146,16);
```

```
  };
  Gap (5,2);
  R_Combine ("Bag 28")
  {
   R_Date("OxA-29459",125,23);
   R_Date("AA103246",128,22);
  };
  Gap (5,2);
  R_Combine ("Bag 29")
  {
   R_Date("OxA-32071 Bag 29",89,24);
   R_Date("OxA-32119   Bag 29",69,24);
  };
  Gap (5,2);
  R_Combine ("Bag 30")
  {    R_Date("OxA-32735",117,25);
   R_Date("AA103248",130,22);
  };
  Gap (5,2);
  R_Date ("Bag 31 OxA-29461",140,23);
  Gap (5,2);
  R_Combine ("Bag 32")
  {
   R_Date("OxA-29462",162,23);
   R_Date("AA103250",162,16);
   R_Date("OxA-29463",121,23);
  };
  Gap (5,2);
  R_Combine ("Bag 33")
  {
   R_Date("OxA-29464",120,23);
   R_Date("AA103251",138,16);
  };
  Boundary ("End");
 };
};
```

Table S7. OxCal (19) runfile for the Tel Rehov dates reported in Fig. 4B. The ^{14}C age values for the 11 stratigraphically ordered archaeological elements listed in Fig. 2 of ref. 31 are analyzed as an ordered sequence. For the data reported in Fig. 4B a first iteration is the published data with IntCal13 (17). Then this runfile is modified with the extra line added of: Delta_R ("Southern Levant Average",19,5); and then a third version was run with the Jordan juniper (JJ) modified approximate calibration curve shown in Fig. 4A.

```
Plot()
 {
  Sequence ("Iteration 1: Bruins et al. 2003 Rehov with IntCal13")
  {
   Boundary ("Start");
   R_Date ("Area D Phase D6a L2836",2928,26);
   R_Date ("Area D Phase D4b L1845 House", 2924,22);
   R_Date ("Area D Phase D4a L1836 Street", 2885,26);
   R_Date ("Area D Phase D3 Pits", 2831,18);
   R_Date ("Area D Phase D2 Locus 1802", 2805,15);
   R_Date ("Area C Stratum VI Locus 4426", 2768,12);
   R_Date ("Area C Stratum V Locus 2441", 2776,9);
   R_Date ("Area C Stratum V Locus 2425", 2788,14);
   R_Date ("Area C Stratum V Locus 2422", 2771,8);
   R_Date ("Area B Stratum V Locus 4218", 2786,22);
   R_Date ("Area C Stratum IV Locus 5498", 2755,25);
   Boundary ("End");
  };
};
```

Table S8. OxCal (19) runfile for the Khirbat en-Nahas ^{14}C data and Bayesian chronological model (32) as reported in Fig. 4B. We ran three versions of the model. Iteration 1 – *without* the yellow highlighted text in line 3 of the runfile below – was the published data and model re-run with IntCal13 (17). Iteration 2 adjusted this model by employing the approximate average Jordanian offset of 19±5 ^{14}C years (see main text) using the yellow highlighted text in line 3 of the runfile below. Iteration 3 in turn considered the situation if the model (*without* the Delta_R line in yellow highlight) was run with the approximate Jordan juniper modified calibration curve shown in Fig. 4A.

```
Plot()
 {
  Delta_R("Jordanian Av. Offset", 19, 5);
  Sequence ()
  {
   Sequence ()
   {
    Boundary ("Start Stratum 3");
    Sequence ("Stratum 3")
    {
     R_Date ("OxA-17646",2871,26);
     R_Date ("OxA-17644",2824,25);
     R_Date ("OxA-17647",2764,25);
     R_Date ("OxA-17643",2813,26);
     R_Date ("OxA-17703",2792,30);
     R_Date ("OxA-17640",2770,25);
     R_Date ("OxA-17642",2781,25);
     R_Date ("OxA-17641",2767,25);
     R_Date ("OxA-17645",2747,25);
    };
    Boundary ("End 3/start Strat 2 building and strat 1 slag mound");
    Phase ()
    {
     Sequence ()
     {
      Boundary ("Start 2");
      Sequence ("Stratum 2 Building")
      {
       R_Date ("OxA-17638",2814,25)
       {
        Outlier();
       };
       R_Date ("OxA-17633",2734,25);
       R_Date ("OxA-17632",2713,26);
       R_Date ("OxA-17636",2732,25);
       Phase ()
       {
        R_Date ("OxA-17635",2777,25);
        R_Date ("OxA-17634",2783,25);
       };
       R_Date ("OxA-17702",2740,30);
       R_Date ("OxA-17631",2676,26)
       {
        Outlier();
       };
```

```
    };
    Boundary ("End 2");
   };
   Sequence ()
   {
    Boundary ("Start 1");
    Sequence ("Stratum 1")
    {
     R_Date ("OxA-17639",2678,26);
     R_Date ("OxA-17637",2836,26)
     {
      Outlier();
     };
     R_Date ("OxA-12437",2746,35);
     R_Date ("OxA-12436",2659,32)
     {
      Outlier();
     };
     R_Date ("OxA-17630",2676,26);
    };
    Boundary ("End 1");
   };
  };
  Boundary ("End Sequence");
 };
};
};
```

Supplementary References

1. Daher RF (2007) Reconceptualizing Tourism in the Middle East: Place, Heritage, Mobility and Competitiveness. *Tourism in the Middle East: Community, Change and Transformation*, ed Daher RF (Tourism and Cultural Change 9, Channel View Publications, Clevedon), pp. 1-69.

2. Schweingruber FH (1988) *Tree Rings: Basics and Applications of Dendrochronology* (D. Reidel, Dordrecht).

3. Cook ER, Kairiukstis LA, Eds. (1990) *Methods of Dendrochronology: Applications in the Environmental Sciences* (Kluwer, Dordrecht).

4. Speer JH (2010) *Fundamentals of Tree Ring Research* (University of Arizona Press, Tucson).

5. Brewer PW (2014) Data Management in Dendroarchaeology Using Tellervo. *Radiocarbon* 56: 79-83.

6. Harris K (2007) Corina 1.1. 2007 version of a 2003 release. Available: http://dendro.cornell.edu/corina/download.php.

7. Holmes RL (1983) Computer-assisted quality control in tree-ring dating and measurement. *Tree-Ring Bulletin* 43: 69-78.

8. Touchan R, Meko D, Hughes MK (1999) A 396-year reconstruction of precipitation in southern Jordan. *Journal of the American Water Resources Association* 35: 49-59.

9. Touchan R, Hughes MK (1999) Dendrochronology in Jordan. *J. Arid Environments* 42: 291-303.

10. Jull AJT, et al. (2006) Application of accelerator mass spectrometry to environmental and paleoclimate studies at the University of Arizona. *Radionuclides in the Environment*, eds Povinec PP, Sanchez-Cabrera JA (Radioactivity in the Environment 8, Elsevier, Amsterdam), pp 3-23.

11. Jull AJT, et al. (2008) Accelerator mass spectrometry of long-lived light radionuclides. *Analysis of Environmental Radionuclides,* ed Povinec PP (Radioactivity in the Environment 11, Elsevier, Amsterdam), pp 241-262.

12. Gaudinski JB, et al. (2005) Comparative Analysis of Cellulose Preparation Techniques for Use with ^{13}C, ^{14}C, and ^{18}O Isotopic Measurements. *Analytical Chemistry* 77: 7212-7224.

13. Brock F, Higham TFG, Ditchfield P, Bronk Ramsey C (2010) Current pretreatment methods for AMS radiocarbon dating at the Oxford Radiocarbon Accelerator Unit (ORAU). *Radiocarbon* 52: 103-112.

14. Staff RA, Reynard L, Brock F, Bronk Ramsey C (2014) Wood Pretreatment Protocols and Measurement of Tree-Ring Standards at the Oxford Radiocarbon Accelerator Unit (ORAU). *Radiocarbon* 56: 709-715.

15. Bronk Ramsey C, Higham T, Leach P (2004) Towards high-precision AMS: progress and limitations. *Radiocarbon* 46: 17-24.

16. Southon JR, Magana AL (2010) A Comparison of Cellulose Extraction and ABA Pretreatment Methods for AMS ^{14}C Dating of Ancient Wood. *Radiocarbon* 52: 1371-1379.

17. Reimer PJ, *et al*. (2013) IntCal13 and Marine13 Radiocarbon Age Calibration Curves 0-50,000 Years Cal BP. *Radiocarbon* 55: 1869-1887.

18. Ward GK, Wilson SR (1978) Procedures for comparing and combining radiocarbon age determinations: a critique. *Archaeometry* 20: 19-31.

19. Bronk Ramsey C (2009) Bayesian analysis of radiocarbon dates. *Radiocarbon* 51: 337-360.

20. Hoper ST, McCormac FG, Hogg AG, Higham TFG, Head MJ (1998) Evaluation of Wood Pretreatments on Oak and Cedar. *Radiocarbon* 40: 45-50.

21. Bronk Ramsey CB, *et al*. (2010) Radiocarbon-based chronology for dynastic Egypt. *Science* 328: 1554-1557.

22. Bronk Ramsey C, et al. (2002) Radiocarbon dates from the Oxford AMS System; Archaeometry Datelist 31. *Archaeometry* 44 Supplement 1: 1-149.

23. Tyers, C, et al. (2009) Wiggle-Matching Using Known-Age Pine from Jermyn Street, London. *Radiocarbon* 51: 385-396.

24. Bayliss A, et al. (2017) Informing Conservation: Towards ^{14}C Wiggle-Matching of Short Tree-Ring Sequences from Medieval Buildings in England. *Radiocarbon* 59: 985-1007.

25. Manning SW, et al. (2013) Radiocarbon Calibration in the Mid to Later 14th Century BC and Radiocarbon Dating Tell el-Amarna, Egypt. *Radiocarbon and the Chronologies of Ancient Egypt*, eds Shortland AJ, Bronk Ramsey C (Oxbow Books, Oxford), pp.121-145.

26. Staff RA, et al. (2011) New ^{14}C Determinations from Lake Suigetsu, Japan: 12,000 to 0 Cal BP. *Radiocarbon* 53: 511-528.

27. Hogg A, *et al.* (2016) Punctuated Shutdown of Atlantic Meridional Overturning Circulation during Greenland Stadial 1. *Scientific Reports* 6:25902; doi: 10.1038/srep25902.

28. Jull AJT, et al. (2014) Excursions in the ^{14}C record at A.D. 774–775 in tree rings from Russia and America. *Geophys. Res. Lett.* 41: 3004-3010.

29. Miyake F, et al. (2017) Large ^{14}C excursion in 5480 BC indicates an abnormal sun in the mid-Holocene. *Proc. Natl. Acad. Sci. U.S.A.* 114: 881-884.

30. Donahue DJ, Linick TW, Jull AJT (1990) Isotope-ratio and background corrections for accelerator mass spectrometry radiocarbon measurements. *Radiocarbon* 32: 135-142.

31. Burr GS, et al. (2007) Error analysis at the NSF Arizona AMS Facility. *Nuclear Instr. Meth. Phys. Res* B. 259: 149-153.

32. Bruins HJ, van der Plicht J, Mazar A (2003) ^{14}C dates from Tel Rehov: Iron Age chronology, pharaohs, and Hebrew kings. *Science* 300: 315-318.

33. Levy TE, *et al*. (2008) High-precision radiocarbon dating and historical biblical archaeology in southern Jordan. *Proc. Natl. Acad. Sci. U.S.A.* 105: 16460-16465.

34. Felis T, et al. (2000) A coral oxygen isotope record from the northern Red Sea documenting NAO, ENSO, and North Pacific teleconnections on Middle East climate variability since the year 1750. *Paleoceanography* 15: 679-694.

35. Xing P, *et al*. (2016) The Extratropical Northern Hemisphere Temperature Reconstruction during the Last Millennium Based on Novel Method. *PLoS ONE* 11(1): e0146776.

36. Vaquero JM, Trigo RM (2015) Redefining the limit dates for the Maunder Minimum. *New Astronomy* 34: 120-122.

37. Nicault A, *et al*. (2008) Mediterranean drought fluctuation during the last 500 years based on tree-ring data. *Climate Dynamics* 31: 227-245.

38. Moberg A, Sonechkin DM, Holmgren K, Datsenko NM, Karlén W (2005) Highly variable Northern Hemisphere temperatures reconstructed from low- and high-resolution proxy data. *Nature* 433: 613-617.

39. Schneider L, *et al*. (2015) Revising midlatitude summer temperatures back to A.D. 600 based on a wood density network. *Geophysical Research Letters* 42: 4556-4562.

40. Wilson R, *et al*. (2016) Last millennium northern hemisphere summer temperatures from tree rings: Part I: the long term context. *Quaternary Science Reviews* 134: 1-18.

41. Anchukaitis KJ, *et al.* (2017) Last millennium Northern Hemisphere summer temperatures from tree rings: Part II, spatially resolved reconstructions. *Quaternary Science Reviews* 163: 1-22.

42. Mann ME (2002) Large-Scale Climate Variability and Connections with the Middle East in Past Centuries. *Climatic Change* 55: 287-314.

43. Stubbs JH (2009) *Time Honored: A Global View of Architectural Conservation* (John Wiley & Sons, Hoboken).

44. Middleton VTC, Hawkins R (1998) *Sustainable Tourism: A Marketing Perspective* (Routledge, London).

45. Daher RF (1999). Gentrification and the Politics of Power, Capital and Culture in an Emerging Jordanian Heritage Industry. *Traditional Dwellings and Settlements* X (11): 33-45.

46. Nagy S, Abu-Dayyeh N (2002) Village air for urban elites. *Expedition* 44(2): 10-18.

47. Baillie MGL, Pilcher JR (1973) A simple cross-dating program for tree-ring research. *Tree-Ring Bulletin* 33: 7-14.

48. Eckstein D, Bauch J (1969) Beitrag zur Rationalisierung eines dendrochronologischen Verfahrens und zur Analyse seiner Aussagesicherheir. *Forstwissenschaftliches Zentralblatt* 88: 230-250.

49. Buras A, Wilmking M (2015) Correcting the calculation of Gleichläufigkeit. *Dendrochronologia* 34: 29-30 (2015).

50. Hogg AG, *et al*. (2013) SHCal13 southern hemisphere calibration, 0-50,000 years cal BP. *Radiocarbon* 55: 1889-1903.